Potential Energy Surfaces and Dynamics Calculations

for Chemical Reactions and Molecular Energy Transfer

Edited by

Donald G. Truhlar

University of Minnesota
Minneapolis, Minnesota

PLENUM PRESS • NEW YORK AND LONDON

Chapter by B. C. Garrett, D. G. Truhlar, and R. S. Grev, pages 587-637.
1981

DETERMINATION OF THE BOTTLENECK REGIONS OF POTENTIAL ENERGY SURFACES FOR ATOM TRANSFER REACTIONS BY VARIATIONAL TRANSITION STATE THEORY

Bruce C. Garrett*

Department of Chemistry
University of Minnesota
Minneapolis, MN 55455

and

Battelle Columbus Laboratories
505 King Avenue,
Columbus, OH 43201

Donald G. Truhlar and Roger S. Grev†

Department of Chemistry
University of Minnesota
Minneapolis, MN 55455

I. INTRODUCTION

A major difficulty in the calculation of reliable equilibrium rate constants for gas-phase bimolecular reactions is the lack of accurate information about potential energy surfaces. The calculation of accurate, detailed dynamical quantities such as inelastic and reactive cross sections requires a knowledge of the potential energy surface over large regions of the configuration space. Thermal rate constants represent an average of such detailed dynamical quantities, and as a result they are less sensitive to fine features of the surface. Thus accurate thermal rate constants may be calculated using

*Present address: Chemical Dynamics Corporation, 1550 West Henderson Road, Suite N140, Columbus, OH 43220.

†Lando Research Fellow, 1979, 1980. Present address: University of Minnesota, Morris, MN 56267.

less information about the potential surfaces than is required to calculate more detailed quantities; one of the goals of the present chapter is to discuss which regions of the surfaces are most important in controlling the rates of chemical reactions.

Transition-state theory (TST)[1] provides one of the most practical approximation schemes for calculating equilibrium rate constants for thermally activated bimolecular reactions. Conventionally the transition state is defined as a surface in configuration space separating the reactant and product regions and located at the saddle point of the potential energy surface. Applications of TST requires knowledge of the potential energy surface in the saddle point and reactant regions, and the saddle point region is identified as most important in controlling the rate of the reaction.

Generalized transition-state theory (GTST) is an attempt to improve on conventional TST by using phase-space dividing surfaces that separate reactants from products but that are not restricted to be configuration-space surfaces passing through the saddle point. These dividing surfaces are called generalized transition states; in variational transition-state theory (VTST) their optimum locations are determined by a variational criterion.[2-9] VTST calculations require knowledge of wider regions of the potential energy surface than do conventional TST calculations; the variationally determined transition states found by examining this larger portion of the surface are more closely related to the dynamical bottlenecks to reaction than are the conventional transition states.

A concern in using TST or VTST for calculating equilibrium rate constants or locating bottlenecks is the accuracy of the approximations inherent in the theory. Recently there has been great interest in examining and testing the fundamental assumptions of classical mechanical transition-state theory.[7,9-15] (Additional references are given in section II.B.) Classically, the fundamental assumption[16] of GTST is a dynamical one which can be stated as follows: Any trajectory which reaches the generalized transition state and has momentum directed in the product direction is a reactive trajectory. The consequences of this assumption are (i) classical GTST is exact if, and only if, all trajectories cross the generalized transition state only once, and (ii) if recrossing does occur classical GTST overestimates the exact classical equilibrium rate constant.[12] This leads naturally to the variational principle mentioned above in which the generalized transition state is located to give the least upper bound on, and thereby the best estimate of, the exact classical rate.

Conventionally[1] the transition-state assumption has been extended to a quantum mechanical world by assuming a separable reaction-coordinate orthogonal to the dividing surface and quantizing

the bound motions within the dividing surface. The quantized energy levels of the bound degrees of freedom are used for state counting in calculations for microcanonical ensembles or for calculating partition functions in calculations for canonical ensembles. Quantal effects for the motion along the reaction coordinate are included in a multiplicative transmission coefficient, $\kappa(T)$, by calculating quantum mechanical transmission through and across a one-mathematical-dimensional potential barrier. Attempts to obtain a nonseparable quantum mechanical TST (*i.e.*, one which contains no auxiliary assumption besides the fundamental dynamical assumption) have not been totally successful; however, they have led to new insight into the theory.[6,17-19]

A consequence of using the conventional quantization in GTST is that it no longer provides an upper bound on the equilibrium rate constant. Although it cannot be justified by a rigorous variational principle, we have nevertheless employed the conventional quantization procedure and chosen the generalized transition state location as the one that minimizes the rate calculated with $\kappa(T) = 1$. Then we have estimated $\kappa(T)$. This procedure has been tested empirically on collinear model reactions for several potential energy surfaces[20-26] and for reactions in three dimensions with an accurate potential energy surface.[27,28] Comparisons to experiment are complicated by uncertainties in the potential energy surfaces so the most definitive tests have been comparisons of conventional TST and VTST for assumed but realistic potential surfaces to accurate quantal rate constants for the same surfaces.[21-26,28] For the one case where an accurate analytic potential surface is available[29-31] both conventional TST and VTST have been compared to experimental results.[27,28] In general this VTST procedure has proved to be quite reliable; this work has been reviewed elsewhere[32] and the conclusions are summarized in section II.B.

In this chapter, the emphasis is on the use of VTST to help identify the regions of potential energy surfaces that are most important in determining reliable rate constants. Two approaches have been used to date. One is to study a wide variety of model potential energy surfaces to predict general trends for various reaction types.[33-35] A second method is to use model potential energy surfaces that have been adjusted so that dynamical predictions agree as well as possible with experimental results.[36] Such approaches can be used to locate those regions of the potential energy surface which should be studied more carefully by electronic structure calculations. In this paper we use the former approach and we report many new calculations as well as reviewing some aspects of our previous ones.

Another subject discussed in this chapter is the relationship between classical and quantum mechanical rate calculations; see especially sections II.B and IV. This is of interest since there

has been more work done on classical GTST than on the quantized version; we shall see, however, that the bottleneck may be quite different for the classical and quantal versions of the same reaction at the same temperature. This difference occurs because the typical contribution to a classical reaction rate at temperature T comes from energies within a few kT above the classical barrier height, whereas for most of the reactions we have studied the accurate quantum mechanical reaction rate is very small at such an energy because quantal systems involving hydrogens tend to have more than kT of energy tied up in bound vibrational motions throughout the whole reaction.

II. THEORY

A. Quantized Formulation, Including Tunneling

The quantum mechanical VTST formalism used for the rate-constant calculations presented here is described in detail elsewhere.[22,23,27,33] Here we present a brief review of the theory.

We work in a mass-scaled coordinate system in which the kinetic energy term is diagonal and each term has the samd reduced mass μ, which is the reduced mass for the relative motion of the reactants. The minimum-energy path (MEP) is defined as the path of steepest descents from the saddle point to both reactants and products in this coordinate system. Distance from the saddle point along the minimum-energy path in this coordinate system is the reaction coordinate s. By definition s equals zero at the saddle point and is less than zero on the reactant side of the saddle point. The generalized transition states are defined to be orthogonal to the MEP and are specified by the location s at which they cross the MEP.

The generalized-transition-state-theory microcanonical rate constant is a function of the total energy E and the location of the transition state; it is given by

$$k^{GT}(E,s) = N^{GT}(E,s)/h\phi^{R}(E) \tag{1}$$

where h is Planck's constant and $\phi^{R}(E)$ is the reactant density of states per unit energy per unit volume. $N^{GT}(E,s)$ is the generalized TST cumulative reaction probability, or sum of states, defined by

$$N^{GT}(E,s) = \sum_{\underset{\sim}{\alpha}} \theta[E - V_a(\underset{\sim}{\alpha},s)] \tag{2}$$

where $\theta(x)$ is a Heaviside function, $V_a(\underset{\sim}{\alpha},s)$ is an adiabatic potential curve

$$V_a(\underset{\sim}{\alpha},s) = V_{MEP}(s) + \varepsilon_{int}(\underset{\sim}{\alpha},s) \tag{3}$$

and $\underset{\sim}{\alpha}$ denotes the set of quantum numbers of all the internal modes (vibrational and rotational) orthogonal to the MEP. $V_{MEP}(s)$ is the potential energy along the minimum-energy path, and $\varepsilon_{int}(\underset{\sim}{\alpha},s)$ is the local vibrational-rotational energy for motion normal to the MEP with internal quantum numbers $\underset{\sim}{\alpha}$. The GTST cumulative reaction probability is the number of energetically available internal states of the generalized transition state at s. In conventional TST the transition state is located at the saddle point, *i.e.*, at s = 0, and the microcanonical rate constant is denoted $k^{\ddagger}(E)$. In VTST applied to a microcanonical ensemble, *i.e.*, microcanonical variational theory (μVT), the generalized transition state is located to minimize the number of states $N^{GT}(E,s)$ and thereby minimize the rate constant $k^{GT}(E,s)$, with the resulting minimum values being called $N^{\mu VT}(E)$ and $k^{\mu VT}(E)$. Therefore the μVT transition-state location depends on the energy and is denoted $s_*^{\mu VT}(E)$. The number of internal states depends on the value of the classical potential energy along the MEP, the widths of the vibrational wells orthogonal to the MEP, and the moments of inertia of the generalized transition state species. As the dividing surface is moved towards the saddle point $V_{MEP}(s)$ increases and, if the channel width did not increase, the number of energetically available states would always decrease. But an increase in the width of one or more vibrational wells can cause $N^{GT}(E,s)$ to increase. In conventional TST only the classical energetic criterion based on $V_{MEP}(s)$ is considered for locating the transition state; thus it is located at the saddle point where $V_{MEP}(s)$ is maximum. In μVT the location of the dividing surface is determined by a competition between this energetic criterion and the "entropic" effects of the bound degrees of freedom.

The canonical, *i.e.*, thermal, rate constant of μVT can be obtained by Boltzmann averaging the energy-dependent rate constants; the result is called $k^{\mu VT}(T)$. One can also define a GTST canonical rate constant which is a function of the temperature T and the location of the dividing surface, and which is given by

$$k^{GT}(T,s) = \sigma \frac{k_B T}{h} \frac{Q^{GT}(T,s)}{\phi^R(T)} \exp[-\beta V_{MEP}(s)] \tag{4}$$

where σ is a statistical symmetry factor (see reference 33), k_B is Boltzmann's constant, $\phi^R(T)$ is the reactant's partition function per unit volume, and $\beta = (k_B T)^{-1}$. The GTST partition function is

$$Q^{GT}(T,s) = \sum_{\underset{\sim}{\alpha}} \exp[-\beta \varepsilon_{int}(\underset{\sim}{\alpha},s)] \tag{5}$$

In VTST applied to a canonical ensemble, *i.e.*, canonical variational theory (CVT), the dividing surface is located to minimize the thermal rate constant $k^{GT}(T,s)$. This location is a function of the temperature T and is denoted $s_*^{CVT}(T)$. The conventional TST choice of dividing surface corresponds to minimizing only the exponential factor in equation (4), whereas the CVT rate constant, $k^{CVT}(T)$, is determined such that both the energetic factor, the exponential, and the entropic factor, the partition function, are included in the minimization procedure.

In μVT the lowest energy that can contribute to the thermal rate constant $k^{\mu VT}(T)$ is equal to the maximum V^{AG} of the ground-state adiabatic potential curve $V_a^G(s)$ [$\equiv V_a(\alpha=G,s)$, where $\alpha=G$ denotes the ground state and zero angular momentum].[23,27] For energies below this threshold, the dividing surface can be placed at the location of the maximum and $N^{GT}(E,s)$ will be zero. In CVT, only one dividing surface is chosen at each temperature and this surface is not necessarily located at the top of the ground-state adiabatic barrier. Therefore, energies which are lower than the μVT threshold can contribute to the thermal rate constant $k^{CVT}(T)$. This deficiency is removed in the improved canonical variational theory (ICVT) by chosing two dividing surfaces: one located at the maximum of $V_a^G(s)$ for all energies lower than the adiabatic barrier height, and the other chosen for each temperature to be the best compromise to minimize the contributions of all higher energies to the thermal rate constant at that temperature.[23]

The rate constants $k^{\mu VT}(T)$, $k^{ICVT}(T)$, $k^{CVT}(T)$, and $k^{\ddagger}(T)$ are all calculated from the quantized energy levels $\epsilon_{int}(\underline{\alpha},s)$ of the bound degrees of freedom; however, the reaction-coordinate motion is treated classically in the calculation of these four quantities. Corrections for quantal motion along the reaction coordinate can be included by multiplying the canonical rate constants by an approximate transmission coefficient $\kappa(T)$. Except for one study[37,38] in which no separation of variables was made, all attempts to include the remaining quantal effects have involved the quantal calculation of motion over and through one-mathematical-dimensional potential barriers. The simplest tunneling factor for transition-state theory is that proposed by Wigner[39] in which the transmission coefficient is the leading quantal correction to conventional TST to lowest order in $\hbar$. The resulting corrected canonical rate constant is

$$k^{\ddagger/W}(T) = \kappa^{W}(T)\, k^{\ddagger}(T) \tag{6}$$

where

$$\kappa^{W}(T) = 1 + (\hbar|\omega^{\ddagger}|/k_B T)^2/24 \tag{7}$$

and $\omega^{\ddagger}$ is the imaginary frequency for the unbound normal mode at the saddle point. Although the conditions for the validity of the assumptions made in obtaining this factor are seldom satisfied,[6,21] it is used often because of its simplicity. Use of this transmission coefficient requires a knowledge of the potential energy surface only in the vicinity of the saddle point.

The vibrationally adiabatic model provides a framework for including quantal effects on reaction-coordinate motion that is more consistent with VTST.[40] In the adiabatic theory of reactions[41] state-selected rate constants are calculated for each set of internal quantum numbers $\underset{\sim}{\alpha}$. The adiabatic approximation is used to construct the effective potentials $V_a(\underset{\sim}{\alpha},s)$ for the one-dimensional motion from reactants to products. For classical reaction-coordinate motion of a system initially in quantum state $\underset{\sim}{\alpha}$, reaction occurs if the system has enough total energy to surmount the maximum $V^A(\underset{\sim}{\alpha})$ of $V_a(\underset{\sim}{\alpha},s)$ as a function of s. The thermal rate constant, $k^A(T)$, is the appropriate thermal average of the state-selected rate constants, $k^A(\underset{\sim}{\alpha},T)$. If the same approximations are used in computing $N^{GT}(E,s)$ and $\epsilon_{int}(\underset{\sim}{\alpha},s)$ in both the adiabatic theory of reactions with classical reaction-coordinate motion and μVT, then they are equivalent.[22] Since quantum effects are most important at low energies where contributions to the thermal rate constant from the ground state predominate, the treatment of the threshold energy region is improved by using a vibrationally adiabatic ground-state transmission coefficient

$$\kappa^{VAG}(T) = \frac{k^{VA}(\underset{\sim}{\alpha}=G,T)}{k^{A}(\underset{\sim}{\alpha}=G,T)} \tag{8}$$

and $k^{VA}(\underset{\sim}{\alpha}=G,T)$ is the state-selected rate constant for quantal motion on the one-dimensional adiabatic ground-state potential curve, and $k^A(\underset{\sim}{\alpha}=G,T)$ is the same quantity with reaction-coordinate motion treated classically. This transmission coefficient is then used multiplicatively to define a corrected prediction for the thermally averaged μVT rate constant.

$$k^{\mu VT/VAG}(T) = k^{\mu VT}(T)\,\kappa^{VAG}(T) \tag{9}$$

Thus we see that at low temperatures $k^{\mu VT/VAG}(T) \to k^{VA}(\underset{\sim}{\alpha}=G,T)$, while at high temperatures $\kappa^{VAG}(T) \to 1$ and it no longer matters that the transmission coefficient is based on the ground state.

Care was taken to insure that the threshold of the ICVT is the same as the threshold for the μVT. Therefore $k^{ICVT}(T) \to k^A(\underset{\sim}{\alpha}=G,T)$ at low temperature and we can also use $\kappa^{VAG}(T)$ with the ICVT rate constant. This yields the corrected prediction

$$k^{ICVT/VAG}(T) = k^{ICVT}(T)\,\kappa^{VAG}(T) \tag{10}$$

so that $k^{ICVT/VAG}(T) \to k^{VA}(\underset{\sim}{\alpha}=G,T)$ at low T.

The use of quantal adiabatic transmission coefficients with CVT and conventional TST is not as straightforward because the thresholds for these theories are not the same as the adiabatic threshold. We can define the correct transmission coefficient to be used with conventional TST as[23,27,40,42]

$$\kappa^{\ddagger/VAG}(T) = \frac{\int_0^\infty P^{VAG}(E)\, e^{-\beta E}\, dE}{\int_{V_a^G(s=0)}^\infty e^{-\beta E}\, dE} \tag{11}$$

where $P^{VAG}(E)$ is the transmission probability for the one-dimensional vibrationally adiabatic ground-state potential curve $V_a^G(s)$ for total energy E. The corrected rate constant may be written

$$k^{\ddagger/VAG}(T) = k^{\ddagger}(T)\,\kappa^{\ddagger/VAG}(T) \tag{12}$$

Similar considerations for CVT lead to

$$\kappa^{CVT/VAG}(T) = \frac{\int_0^\infty P^{VAG}(E)\, e^{-\beta E}\, dE}{\int_{V_a^G[s=s_*^{CVT}(T)]}^\infty e^{-\beta E}\, dE} \tag{13}$$

where $s_*^{CVT}(T)$ is the location of the CVT transition state and[23,27]

$$k^{CVT/VAG}(T) = k^{CVT}(T)\,\kappa^{CVT/VAG}(T) \tag{14}$$

We can rewrite equation (11) as[23]

$$\kappa^{\ddagger/VAG}(T) = \kappa^{\ddagger/CAG}(T)\,\kappa^{VAG}(T) \tag{15}$$

where $\kappa^{\ddagger/CAG}(T)$ is a classical transmission coefficient which accounts for the difference in the thresholds of μVT and conventional TST

$$\kappa^{\ddagger/CAG}(T) = \exp\{-\beta[V^{AG} - V_a^G(s=0)]\} \tag{16}$$

Similar considerations for CVT lead to

$$\kappa^{CVT/CAG}(T) = \kappa^{CVT/CAG}(T)\,\kappa^{VAG}(T) \tag{17}$$

where

$$\kappa^{CVT/CAG}(T) = \exp\left(-\beta\{V^{AG} - V_a^G[s_*^{CVT}(T)]\}\right) \tag{18}$$

By using $\kappa^{\ddagger/CAG}(T)$ with $k^{\ddagger}(T)$ one obtains

$$k^{\ddagger/CAG}(T) = k^{\ddagger}(T)\,\kappa^{\ddagger/CAG}(T) \tag{19}$$

This corrects for the fact that conventional TST has an effective threshold of $V_a^G(s=0)$ whereas $k^{\mu VT}(T)$ has V^{AG} as its threshold. This correction factor therefore contains a VTST effect since in the low-temperature limit $k^{\ddagger/CAG}(T) \to k^{\mu VT}(T)$. This shows that by using adiabatic transmission coefficients with conventional TST one includes some of the effects of variationally optimizing the location of the dividing surface. Similarly we can define

$$k^{CVT/CAG}(T) = k^{CVT}(T)\,\kappa^{CVT/CAG}(T) \tag{20}$$

We have found[23-26] that $k^{CVT/CAG}(T)$ is usually very similar to k^{ICVT}. As a consequence $k^{CVT/VAG}(T)$ is usually very similar to the more complicated $k^{ICVT/VAG}(T)$.

Use of adiabatic transmission coefficients requires a much wider knowledge of the potential energy surface than does use of the simpler Wigner correction factor. However, the required information is precisely that needed to perform a VTST calculation; namely: (i) the MEP and the potential energy along the MEP and (ii) the vibrational wells normal to the MEP. The recent development of techniques to evaluate the gradient of the potential energy surface in an *ab initio* electronic structure calculation can provide the MEP.[43] There are also efficient algorithms to determine the second derivative matrix of the potential energy surface with respect to the nuclear coordinates.[44] The matrix of second derivatives along the MEP would provide a harmonic approximation to the bound degree of freedom normal to the MEP. In our calculations we also include anharmonicity.[9,33,45] In the applications of the theory that we present here we have obtained such potential energy surface information from a modified and extended BEBO model[33,34] and also from analytic potential energy surfaces which are semiempirical or fit to accurate *ab initio* information. To calculate energy levels and partition functions we approximate the vibrational wells for stretching motions by using Morse potential energy

curves fit to reproduce the second derivative at their minimum and the dissociation energy,[9] and we approximate the vibrational wells for bends by using a harmonic-plus-quartic approximation.[33,45]

B. Tests of the Fundamental Assumption and the Tranmission Coefficients

Variational transition state theory was originally formulated as a purely classical theory.[2-5] Furthermore, it is only for a purely classical world that variational transition-state theory is rigorously justified, *i.e.*, as discussed in section I, classical variational transition state theory does yield an upper bound on the exact classical equilibrium rate constant, but when quantal effects are included there is no bound principle.[46] Although quantal effects like zero point energy and tunneling are very important for thermal rate constants, there is much fundamental interest in purely classical transition state theory.* Thus the formalism of the classical theory has undergone further development,[6-9,15,17,47-59†] and the accuracy of classical transition state theory has been tested by comparison to exact classical dynamics. The tests have involved studies of the trajectory distributions in the interaction region,[10,11,59-61] finding the energy limit up to which the classical theory is exact,[9,12,13,15,52,62,63] and comparing reaction probabilities and rate constants calculated by both conventional TST[7,9-11,13-15,57,64] and VTST[7,9,15,55,57,64,65] to exact classical ones. Section IV discusses the difficulty of extending the conclusions based on these comparisons to the quantum mechanical world. In our own applications of VTST to bimolecular reactions we have also used the "quantum mechanical" formulation of section II.A in which internal states are quantized (quasiclassically) and tunneling effects are included (quantum mechanically or semiclassically). We have compared the rate constants calculated by our quantized formulation, with and without tunneling corrections, to accurate quantum mechanical equilibrium rate constants for the same assumed potential energy surfaces for several collinear reactions[20-26] and one three-dimensional reaction.[28] This work, reviewed elsewhere,[32] shows that: (i) VTST, even when quantal effects are included, although not based on a rigorous bound, still provides considerable improvement in accuracy over conventional transition-state theory in many cases, *i.e.*, the variational procedure is still useful. (ii) VTST, including quantal or semiclassical vibrationally adiabatic transmission coefficients, usually yields good absolute accuracy for the calculation of

*In classical transition-state theory the partition functions become phase space integrals (as compared to state sums in the quantized version).

†References to related work are given in references 8 and 9.

thermal rate constants in a quantum mechanical world. (iii) Consistent incorporation of quantal effects on reaction-coordinate motion in conventional TST by using the vibrationally adiabatic ground-state potential energy curve gives similar results at low temperature to incorporating quantal reaction-coordinate motion in a full variational calculation. We have also compared the results of the quantized theory without tunneling to quasiclassical trajectory calculations.[20,23]

C. Unimolecular Reactions

Quantization effects have also been included in VTST, or similar formalisms, for the study of unimolecular reactions.[67-69] Most of the considerations in the present chapter would also apply to unimolecular reactions. For example, bimolecular reactions with negligible intrinsic barriers (small $V^{\ddagger} - V^{P}$ for endoergic reactions in the notation introduced below) are similar in many respects to simple bond-fission or bond-fusion reactions. In the rest of this chapter though we will explicitly consider only bimolecular reactions.

III. POTENTIAL ENERGY SURFACES AND ENERGETIC QUANTITIES

We shall present results for several kinds of potential energy surfaces. Many of the surfaces are obtained by the London-Eyring-Polanyi-Sato (LEPS) method, involving a single adjustable (Sato) parameter, or by the extended LEPS method, in which different Sato parameters are used for different atomic pairs. These methods are reviewed elsewhere.[70,71] For other calculations we used rotated Morse curves (RMC),[66,72,73] semiempirical valence bond (VB)[74,75] surfaces, and rotated-Morse-bond-energy-bond-order (RMBEBO)[33,34] surfaces.

The RMBEBO formalism is our own extended and modified version of the bond-energy-bond-order (BEBO) method of Johnston and Parr[76] and the reduced-variable-bond-energy-bond-order (RVBEBO) method of Mayer *et al.*[77] The RMBEBO method predicts different saddle point properties than the BEBO and RVBEBO methods, except for symmetric reactions. Unlike those methods, however, it dissociates to correct diatomic limits so that

$$\lim_{s \to -\infty} \varepsilon_{int}(\underset{\sim}{\alpha},s) = \varepsilon^{R}(\underset{\sim}{\alpha}) \tag{21}$$

$$\lim_{s \to +\infty} \varepsilon_{int}(\underset{\sim}{\alpha},s) = \varepsilon^{P}(\underset{\sim}{\alpha}) \tag{22}$$

where $\varepsilon_{int}(\underset{\sim}{\alpha},s)$ is defined below equation (3), and $\varepsilon^R(\underset{\sim}{\alpha})$ and $\varepsilon^P(\underset{\sim}{\alpha})$ are reactant and product energy levels, respectively. For the RMBEBO surfaces we use the diatomic parameters of Johnston and Parr[76] when available, and otherwise those of reference 45. The RMBEBO method is a model for transfer of H between saturated doublet fragments as in CH_3-H-OH rather than between atoms as in C-H-O. Thus, *e.g.*, Johnston and Parr use an H-O bond strength of 114.7 kcal/mol, as compared to the diatomic value of 106.6 kcal/mol. Except where indicated otherwise though we use the mass of the most common atomic isotope, as we do for the calculations with other kinds of surfaces. The RMBEBO surfaces are really model systems that illustrate the kinds of effects that could occur in selected real systems, but a given RMBEBO surface does not represent a specified real system except nominally.

In the rest of this chapter we put the zero of energy at the classical equilibrium potential of reactants. Hence the VAG barrier height ΔV^{AG} is the maximum V^{AG} of the VAG potential curve minus the reactant zero-point energy ε_0^R [$= \varepsilon^R(\underset{\sim}{\alpha}=G) = \varepsilon^{RG}$]. The delta denotes changing the zero of energy to ε_0^R. In other work[23] we have also introduced a convention whereby a tilde refers to changing the zero of energy to the local zero-point energy. Using the definition in equation (3), we can summarize our conventions for barrier quantities as follows:

$$V_{MEP}(s=-\infty) = 0 \tag{23}$$

$$V^{\ddagger} = V_{MEP}(s=0) \tag{24}$$

$$V^P = V_{MEP}(s=\infty) \tag{25}$$

$$V_a(\underset{\sim}{\alpha},s=-\infty) = \varepsilon^R(\underset{\sim}{\alpha}) \tag{26}$$

$$V^A(\underset{\sim}{\alpha}) = \max_s V_a(\underset{\sim}{\alpha},s) \tag{27}$$

$$V^{AG} = V^A(\underset{\sim}{\alpha}=G) \tag{28}$$

$$V_a(\underset{\sim}{\alpha},s=\infty) = \varepsilon^P(\underset{\sim}{\alpha}) \tag{29}$$

$$\Delta V_a(\underset{\sim}{\alpha},s) = V_a(\underset{\sim}{\alpha},s) - \varepsilon^R(\underset{\sim}{\alpha}) \tag{30}$$

$$\Delta V_a^G(s) = \Delta V_a(\underset{\sim}{\alpha}=G,s) \tag{31}$$

$$\Delta E_0 = \Delta V_a^G(s=\infty) \tag{32}$$

$$\tilde{V}_a(\underset{\sim}{\alpha},s) = V_a(\underset{\sim}{\alpha},s) - V_a(\underset{\sim}{\alpha}=G,s) \tag{33a}$$

$$= \Delta V_a(\underset{\sim}{\alpha},s) - \Delta V_a(\underset{\sim}{\alpha}=G,s) \tag{33b}$$

$$= \varepsilon_{int}(\underset{\sim}{\alpha},s) - \varepsilon_{int}(\underset{\sim}{\alpha}=G,s) \tag{33c}$$

Notice that V^P is the classical endoergicity and ΔE_0 is quantal ground-state endoergicity. It is also convenient to define the conventional-transition-state-theory approximation to the barrier height of the vibrationally adiabatic ground-state potential energy curve

$$\Delta V_a^{\ddagger G} = \Delta V_a^G(s=0) \tag{34}$$

This is always less than or equal to

$$\Delta V^{AG} = V^{AG} - \varepsilon^R(\underset{\sim}{\alpha}=G) = \max_s \Delta V_a^G(s) \tag{35}$$

which is the true barrier height of the vibrationally adiabatic ground-state potential curve. Notice that $\Delta V_a^{\ddagger G}$ is the conventional-transition-state-theory energy of activation at 0 K and ΔV^{AG} is the variational-transition-state-theory free energy of activation at 0 K.

The parameters[45,76] and some of the features[33-35] of the RMBEBO surfaces are given elsewhere. The classical and quantal-ground-state endoergicities and the vibrationally adiabatic ground-state (VAG) barrier heights for the other surfaces considered in this chapter are summarized in Table 1. This table also gives references[57,66,70,73-90] for the diatomic input data for these surfaces and, where appropriate, for the Sato parameters. Finally, it assigns a unique number to each surface, and these numbers will be used to specify the surfaces in later tables in this chapter.

IV. COLLINEAR REACTIONS, CLASSICAL AND QUANTIZED

From theoretical considerations the important regions of the potential energy surface within the framework of VTST are those in the vicinity of the MEP. Of these regions, the most crucial parts are those around the locations of the variationally determined transition states. The variational transition states are the dividing surfaces with the smallest number of classical recrossings and are therefore called the dynamical bottlenecks of the reaction. In this section we review the effects of variationally optimizing the dividing surface for several collinear reactions on semiempirical

Table 1
Summary of potential energy surfaces[a]

Surface	System A + BC	V^P (kcal/mol)	ΔE_0 (kcal/mol)	ΔV^{AG} (kcal/mol)		Type of surface	Reference for diatomic Morse parameters	Sato parameters			
				collinear	3 dim.			Ref.	AB	BC	AC
1	$H + H_2$	0.0	0.0	5.74	8.88	VB	74				
2	$H + H_2$	0.0	0.0	6.37	8.53	RMC	66				
	$D + D_2$		0.0	7.35	8.85						
	$D + H_2$		-0.83	6.38	8.38						
	$H + D_2$		0.99	7.89	9.52						
3	$^{15}C + H^{15}C$	0.0	0.0	2.10	3.80	ext. LEPS	57	57	0.2	0.2	0.1
	$^{57}C + H^{57}C$		0.0	2.17							
	$^{42}C + H^{42}C$		0.02	2.18							
4	$Cl + H_2$	3.01	1.05	3.58	5.79	ext. LEPS	90	78	0.187	0.167	0.187
	$Cl + D_2$		1.66	4.69	6.19						
	$Cl + T_2$		1.93	5.25	6.47						
	Cl + HD		0.68	4.47	6.08						
	Cl + DH		1.87	4.09	5.94						
5	H + BrH	0.0	0	3.14	3.39	ext. LEPS	70,79	70,79	0.076	0.076	0.225
	H + BrT		1.55	4.66	4.87						
6	$I + H_2$	35.80	32.84	32.84	32.98	VB	75				
7	$I + H_2$	35.82	32.85	32.86	33.57	RMC	73				
8[b]	$F + H_2$	-31.75	-32.09	0.61	1.78	ext. LEPS	26	80	0.167	0.106	0.167
	$F + D_2$		-31.89	0.70	1.54						
9	$H + F_2$	-103.54	-99.0	2.21	2.39	ext. LEPS	81	81	0	-0.35	0
	$D + F_2$		-100.5	2.19	2.33						
	$T + F_2$		-101.2	2.18	2.31						
10	$H + Cl_2$	-48.64	-45.20	2.37	2.49	LEPS	82		0	0	0
	$D + Cl_2$		-46.39	2.36	2.45						
11	I + HI	0.0	0.0	0.26	1.05	ext. LEPS	76	83	0.2	0.2	0.125
12	I + HI	0.0	0.0	0.20	0.94	ext. LEPS	76[c]	83	0.2	0.2	0.125

13	Cl + CH	25.50	22.56	27.88	28.22	LEPS	76		0	0	0
14	Cl + CH	25.50	22.56	22.66	22.71	ext. LEPS	76	78	0.187	0.167	0.187
15	Cl + HF	34.10	32.47	40.37	41.53	LEPS	76		0	0	0
16	Cl + HF	33.93	32.31	32.86	33.77	ext. LEPS	84	84	0	0.2	-0.08
17[d]	Na + ClH	7.38	3.67	8.39	8.56	ext. LEPS	85	85	0	0.1	0.8
18	Br + HCl	16.16	15.76	15.76	16.14	ext. LEPS	86	86	0	0.185	0.33
19	C + HCl	0.90	0.79	20.97	22.74	LEPS	76		0	0	0
20	C + HCl	0.90	0.79	4.03	5.63	ext. LEPS	76	78	0.167	0.187	0.187
21	C + HCl	0.90	0.79	6.51	8.09	ext. LEPS	76	88	0.275	0.103	0.103
22[e]	Na + FH	17.23	12.14	13.73	14.25	ext. LEPS	85	85	0.10	0.20	0.20
23[d]	Na + ^{19}ClH	7.38	3.70	8.36	8.54	ext. LEPS	85	85	0	0.1	0.8
24	T + HR	0.0	0.16	6.61	7.67	LEPS	87	87	0.15	0.15	0.15
25[f]	D + H_2	0.0	0.82	6.52	8.95	fit to *ab initio* surface	31				
	T + HD		-0.30	6.64	8.87						
	T + T_2		0.0	7.91	9.45						
26	O + H_2	2.80	1.88	8.48	10.71	LEPS	89	89	0.0885	0.0885	0.0885
27[g]	Cl + H_2	3.01	1.05	4.60	6.87	ext. LEPS	90	36	0.1445	0.1445	0.0225
	Cl + T_2		1.93	5.57	6.91						
	Cl + HD		0.68	4.77	6.86						
	Cl + DH		1.87	5.04	6.90						

a. see section III for explanation of abbreviations

b. Muckerman's surface no. 5

c. except D_{HI} = 76.8 kcal/mol (reference 83)

d. Polanyi and Sathyamurthy's surface I,IIG

e. Polanyi and Sathyamurthy's surface IIG

f. Liu-Siegbahn-Truhlar-Horowitz surface (references 29-31)

g. surface no. 3 of reference 36

potential energy surfaces. We consider the classical case as well as the quantized ones.

The theory presented in section II is easily simplified for collinear reactions: volume becomes length, α becomes the vibrational quantum number n, and rotations and bends do not occur. For the classical case, n is replaced by a continuous vibrational radial action variable. To distinguish quantities calculated classically from their quantized versions, we put a subscript C on the classical ones. For example $N_C^{GT}(E,s)$ is the classical GTST cumulative reaction probability. To calculate it, the sum in (2) is replaced by the phase space integral that is its classical limit. $N_C^{GT}(T,s)$ has the interpretation that it is the energetically accessible area in phase space of the generalized TST dividing surface divided by Planck's constant. The classical generalized TST microcanonical rate constant is then calculated by

$$k_C^{GT}(E,s) = N_C^{GT}(E,s)/h\phi_C^R(E) \tag{36}$$

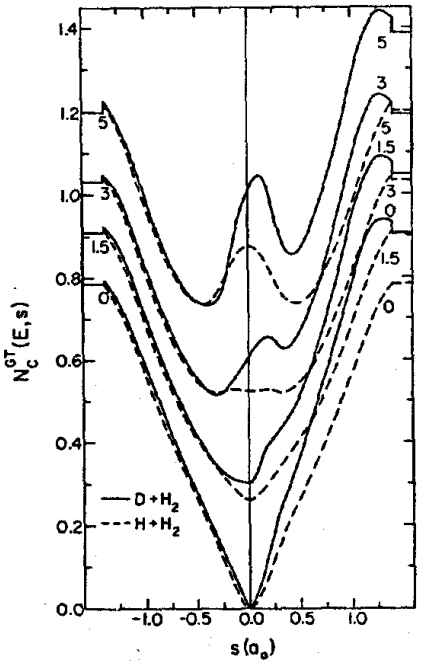

Fig. 1. Generalized-transition-state-theory cumulative reaction probability or sum of states $N_C^{GT}(E,s)$ as a function of reaction coordinate s for collinear $H + H_2 \rightarrow H_2 + H$ and collinear $D + H_2 \rightarrow DH + H$. The curves are labelled at the edges by the energy above the barrier $(E - V^{\ddagger})$ in kcal/mol. The flat sections at both sides are the asymptotic values for $s = \pm\infty$.

where $\phi_C^R(E)$ is the classical limit of $\phi^R(E)$.

Most tests of the fundamental assumptions of classical TST have been for collinear reactions.[9-15] For reactions with high barriers classical TST is a very good approximation to exact classical dynamics for energies just above the saddle point energy. In Fig. 1, we have plotted the classical generalized-transition-state-theory cumulative reaction probability $N_C^{GT}(E,s)$ as a function of the reaction coordinate for four values of the total energy for the reactions H + H_2 and D + H_2 on the Truhlar-Kuppermann[66] (TK) potential energy surface. This potential energy surface has a symmetric barrier of 9.79 kcal/mol. For the symmetric H + H_2 reaction both the potential along the MEP and the transverse stretching frequency exhibit extrema at the saddle point, thereby guaranteeing an extremum in $N_C^{GT}(E,s)$ as a function of s at s = 0. At low energies this is a minimum. For D + H_2, the minimum of the sum-of-states curve deviates from the saddle point at a much lower energy, 1.5-2 kcal/mol above the barrier, compared to 2.5-3 kcal/mol above the barrier for H + H_2. For both reactions the effect of variationally optimizing the location of the dividing surface is negligible for energies near the classical threshold; however, these variational effects become quite important for D + H_2 at lower energies than for H + H_2. This is illustrated in Fig. 2. The

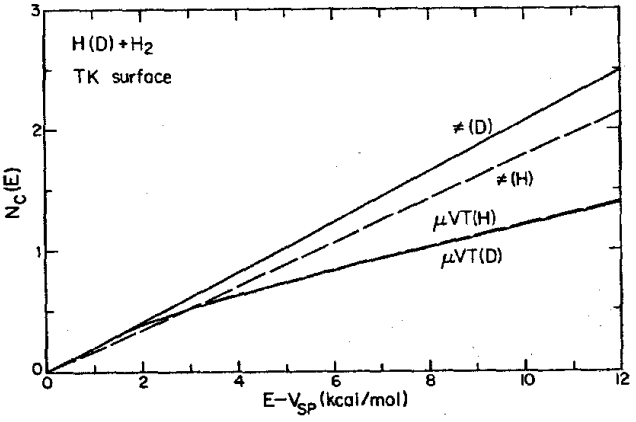

Fig. 2. Cumulative reaction probability for collinear H + H_2 → H_2 + H and collinear D + H_2 → DH + H as a function of energy above the barrier ($E - V^{\ddagger}$). For each reaction the results obtained by conventional transition state theory and microcanonical variational transition state theory are both shown.

quantized generalized-TST sum of states can be obtained from the classical one by the prescription

$$N^{GT}(E,s) = \text{IFIX}\,[N_C^{GT}(E,s) + \tfrac{1}{2}] \tag{37}$$

where IFIX truncates its argument to the next lowest integer. The lowest energy to give a nonzero quantized sum of states at the saddle point will be the energy for which $N_C^{GT}(E,s=0) = \frac{1}{2}$. For H + H_2 this threshold energy is approximately 3.1 kcal/mol above the classical barrier height. At this energy the minimum of the sum-of-states curve has already moved off of the saddle point, but the difference of the sum of states for these two locations is negligible. For D + H_2 the energetic threshold of quantized μVT is about 2.9 kcal/mol above the classical threshold and at this energy the minimum and saddle point values of $N^{GT}(E,s)$ differ considerably. Although variational effects were small for both these reactions in the classical threshold region, the variational effects can be quite large in the quantized threshold region. This behavior is shown in Table 2 for the D + H_2 reaction. For the D + H_2 reaction at 300 K the conventional-TST and μVT rate constants differ only 2% in the classical theory, but differ by a factor of two when the bound degree of freedom is quantized.

A detailed study of the bottleneck regions of the potential energy surface for 24 collinear reactions for a temperature of 300 K is presented in Table 3. Three regions of the potential energy surface are examined: the saddle point ($s = 0$), the maximum ($s = s_*^{AG}$) of the quantized adiabatic ground-state potential curve $V_a^G(s)$, and the quantized CVT transition state at 300 K [$s = s_*^{CVT}(300\ K)$]. The maximum of the ground-state adiabatic potential curve is the variational transition state for energies near threshold. For each dividing surface location the table presents the potential energy on the MEP, the harmonic vibrational frequency (in the form $\hbar\omega_{st}$) for the bound motion normal to the reaction coordinate, and the value of the adiabatic ground-state potential curve. The value of s at the saddle point is zero, and the table gives the values of s at the two other dividing surface locations; in particular $s_*^{CVT}(T)$ is the location of the CVT transition state at temperature T and s_*^{AG} is the location of the VAG barrier maximum. Also included is a ratio of the conventional TST canonical rate constant to the CVT one at 300 K. This ratio is the CVT recrossing correction, *i.e.*, it is the CVT estimate of the correction factor for recrossing of the conventional dividing surface; it is the product of two factors: F_V, which is the ratio of the Boltzmann factor of $V_{MEP}(s)$ at the saddle point to that at the CVT dividing surface, and F_v, which is the ratio of the generalized transition-state vibrational partition function at the saddle point to that at the CVT dividing surface.

Table 2
Classical and quantized canonical rate constants (units of cm molecule^{-1} s^{-1}) for the collinear reaction D + H_2 → DH + H on the TK surface.

T, K	Classical			Quantized		
	$k_C^{\ddagger}(T)$	$k_C^{\mu VT}(T)$	$k_C^{\ddagger}(T)/k_C^{\mu VT}(T)$	$k^{\ddagger}(T)$	$k^{\mu VT}(T)$	$k^{\ddagger}(T)/k^{\mu VT}(T)$
200	2.66×10^{-6}	2.64×10^{-6}	1.01	1.54×10^{-2}	5.50×10^{-3}	2.80
300	1.19×10^{-2}	1.17×10^{-1}	1.02	2.81×10^{0}	1.41×10^{0}	1.99
600	6.20×10^{1}	5.61×10^{1}	1.11	6.05×10^{2}	4.21×10^{2}	1.44
1000	2.13×10^{3}	1.75×10^{3}	1.22	6.21×10^{3}	4.65×10^{3}	1.34
1500	1.35×10^{4}	1.00×10^{4}	1.35	2.32×10^{4}	1.68×10^{4}	1.38
2400	5.85×10^{4}	3.85×10^{4}	1.52	7.37×10^{4}	4.83×10^{4}	1.52
4000	1.72×10^{5}	9.99×10^{4}	1.72	1.87×10^{5}	1.09×10^{5}	1.72
7000	3.85×10^{5}	1.99×10^{5}	1.93	3.96×10^{5}	2.04×10^{5}	1.94

Table 3
Generalized-transition-state quantities for collinear reactions at 300 K.

System A + BC[a]	Surface[b]	Skew angle[c] (degrees)	at saddle point			at maximum of adiabatic ground-state barrier		at CVT transition				comparisons of conventional and canonical variational transition state theory		
			V_{MEP} (kcal/mol)	$\hbar\omega_{str}$ (cm^{-1})	$\Delta V_a^{\ddagger G}$ (kcal/mol)	s_*^{AG} (a_0)	ΔV^{AG} (kcal/mol)	s_*^{CVT} (a_0)	V_{MEP} (kcal/mol)	$\hbar\omega_{str}$ (cm^{-1})	ΔV_a^{CVTG} (kcal/mol)	F_V[d]	F_v[e]	$k^{\ddagger}/k^{CVT}$
H + H_2	1	60.0	9.13	2183	5.94	0	5.94	0	9.13	2183	5.94	1.00	1.00	1.00
H + H_2	2	60.0	9.79	2025	6.37	0	6.37	0	9.79	2025	6.37	1.00	1.00	1.00
D + D_2	2	60.0	9.79	1432	7.35	0	7.35	0	9.79	1432	7.35	1.00	1.00	1.00
D + H_2	2	54.7	9.79	1713	5.97	-0.30	6.38	-0.30	8.38	3038	6.38	0.094	21.17	2.00
H + D_2	2	65.9	9.79	1742	7.79	0.21	7.89	0.21	9.35	2122	7.89	0.48	2.46	1.48
^{15}C + $H^{15}C$	3	20.4	4.49	510	1.13	0.13	2.10	0.13	3.64	1797	2.10	0.24	23.42	5.56
^{57}C + $H^{57}C$	3	10.7	4.49	262	0.87	0.07	2.17	0.06	3.80	1617	2.16	0.31	39.5	12.3
^{42}C + $H^{42}C$	3	11.1	4.49	271	0.89	0.08	2.18	0.08	3.76	1694	2.18	0.29	40.7	11.8
Cl + H_2	4	45.8	7.67	1358	3.42	0.20	3.48	0.19	6.67	2184	3.58	0.19	7.09	1.32
Cl + D_2	4	46.8	7.67	985	4.68	0.015	4.69	0.016	7.66	997	4.68	0.98	1.03	1.01
Cl + T_2	4	47.3	7.67	824	5.25	0.013	5.25	0.013	7.67	833	5.25	0.99	1.02	1.01
Cl + DH	4	55.8	7.67	1252	4.08	-0.018	4.09	-0.18	7.66	1268	4.09	0.98	1.04	1.01
Cl + HD	4	36.4	7.67	1061	3.81	0.18	4.47	0.18	6.81	2138	4.47	0.23	13.0	3.04
H + BrH	5	89.3	3.95	1821	2.78	0.54	3.14	0.54	3.73	2230	3.14	0.70	2.62	1.83
H + BrT	5	88.8	3.95	1487	3.86	0.92	4.66	0.92	3.69	2237	4.66	0.65	5.88	3.84
I + H_2	6	45.2	35.87	1320	31.45	∞	32.84	∞	35.80	2358	32.84	0.90	11.6	10.42
I + H_2	7	45.2	35.88	1291	31.42	∞	32.86	∞	35.82	2358	32.86	0.90	12.4	11.17
F + H_2	8	46.4	1.06	3853	0.31	-0.35	0.61	-0.35	0.88	4204	0.61	0.73	2.27	1.66
F + H_2	8	47.8	1.06	2726	0.53	-0.26	0.70	-0.26	0.95	2934	0.70	0.82	1.63	1.33

$H + F_2$	9	80.9	2.35	787	2.20	-0.03	2.21	-0.03	2.35	793	2.21	0.99	1.01	1.01
$D + F_2$	9	77.4	2.35	771	2.18	-0.05	2.19	-0.05	2.34	785	2.19	0.98	1.04	1.02
$T + F_2$	9	74.8	2.35	763	2.17	-0.06	2.18	-0.06	2.34	783	2.18	0.98	1.05	1.03
$H + Cl_2$	10	83.2	2.40	524	2.37	-0.01	2.37	-0.01	2.42	524	2.37	1.00	1.00	1.00
$D + Cl_2$	10	80.5	2.42	516	2.36	-0.02	2.36	-0.02	2.42	518	2.36	1.00	1.00	1.00

a. reaction occurs with the B end of the diatom

b. see Table 1

c. the angle between the r_{AB} and r_{BC} axes in the (x,y) coordinate system which diagonalizes the kinetic energy

d. $\exp\{-[V_{MEP}(s=0) - V_{MEP}(s=s_*^{CVT})]/k_BT\}$

e. ratio of conventional TST and CVT vibrational partition functions: $Q^{\ddagger}/Q^{CVT}$

As discussed elsewhere,[35] these factors are interpreted classically as showing the competition between the energetic and entropic factors in determining the location of the CVT transition state.

The first three systems are symmetric reactions of $H + H_2$ and $D + D_2$. For these systems there is no effect of variationally optimizing the dividing surface for CVT at 300 K. For the nonsymmetric reactions $D + H_2$ and $H + D_2$ the CVT transition state for 300 K is essentially located at the top of the ground-state adiabatic barrier. This is at a location of $s = -0.30\ a_0$ for $D + H_2$ and $s = 0.21\ a_0$ for $H + D_2$. In moving the dividing surfaces to these locations the potential energy along the MEP drops by 1.41 and 0.44 kcal/mol for $D + H_2$ and $H + D_2$, respectively, but the harmonic frequency for the bound motion increases from 1743 cm^{-1} to 3038 cm^{-1} for $D + H_2$ and from 1742 cm^{-1} to 2122 cm^{-1} for $H + D_2$. The larger increase in the $D + H_2$ vibrational frequency allows the CVT transition state to be moved further from the saddle point and gives a larger decrease of the generalized transition-state theory canonical rate constant. The larger variational effects for $D + H_2$ as compared to $H + D_2$ are an example of a general effect which depends on the mass combination and can be correlated to the skew angle* defined by

$$\beta = \arctan\left[\frac{m_B m_{ABC}}{m_A m_C}\right]^{\frac{1}{2}} \tag{38}$$

The smallest skew angles occur in heavy-atom collisions with a light atom-heavy atom molecule ($H + LH$). Asymptotically the LH pair has a small reduced mass and high vibrational frequency. Consider a symmetric system ($A + BA$) in the r_{AB}, r_{BC} coordinate system. At the symmetric saddle point the transverse stretching motion is just the vibration of the two heavy atoms with the light atom fixed. This motion has a high effective reduced mass and, therefore, a low vibrational frequency. When the potential surface is plotted in scaled and skewed coordinates this drop in frequency at the symmetric saddle point is a widening of the vibrational potential in this region. For systems which are not exactly symmetric the atom in the middle will move at least slightly in the symmetric stretch motion and will affect the reduced mass. However, the qualitative effect is the same. For the $D + H_2$ and $H + D_2$ reactions the skew angles are 54.7° and 65.9°, respectively. Thus, the decrease of the transverse vibrational frequency in going from reactants to the saddle point will be greater for $D + H_2$ than $H + D_2$. The variational optimization of the dividing surface locates the dividing surface away from the saddle

*The skew angle is the angle between the r_{AB} and r_{BC} axes in the scaled and skewed coordinate system that diagonalizes the kinetic energy.[9]

point where this frequency is higher. Although the H + D_2 and D + H_2 reactions are not symmetric they do have a symmetrically located saddle point. For reactions in which the saddle point is not at a symmetric location and which have small skew angles, this dip in the vibrational frequency will be seen in the corner-turning region of the MEP.

The next three systems considered in Table 3 are symmetric or nearly symmetric with extremely small skew angles. These systems are three-body models for H-atom transfer between two rigid alkyl groups. For the three isotopic variants on this potential energy surface we see that as the skew angle decreases the vibrational frequencies at the saddle points drop dramatically; however, the vibrational frequencies for these three systems at the CVT transition states are much

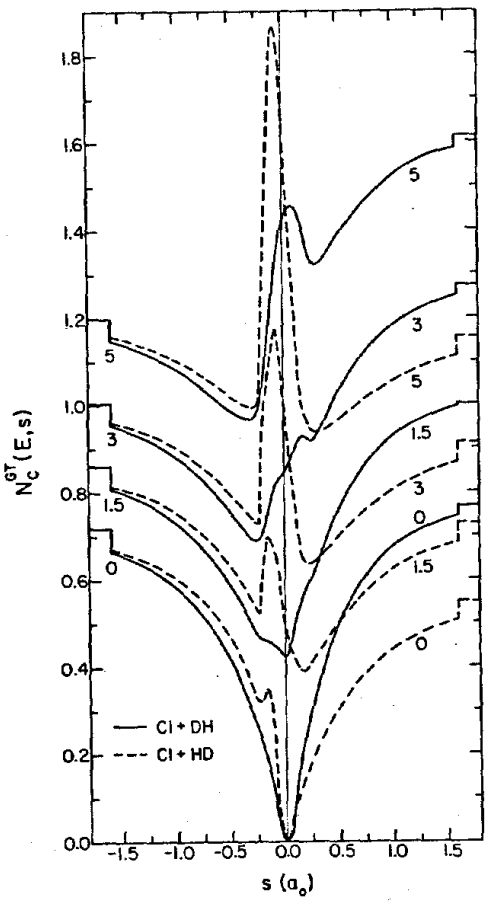

Fig. 3. Same as Fig. 1 except for collinear Cl + HD → ClH + D and collinear Cl + DH → ClD + H.

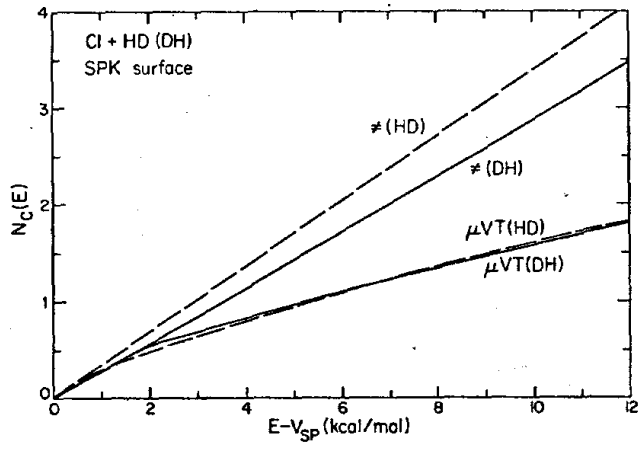

Fig. 4. Same as Fig. 2 except for collinear Cl + HD → ClH + D and collinear Cl + DH → ClD + H.

more similar. For these systems the ratios of the conventional-TST partition functions to the CVT ones are quite large leading to large values of the ratios of conventional TST and CVT rate constants.

The potential energy surface[78] for the Cl + H_2 reaction has a small classical endoergicity of 3.01 kcal/mol and a nearly symmetrically located saddle point. Table 3 contains five isotopic variants of this reaction. The three systems with the highest skew angles Cl + D_2, Cl + T_2, and Cl + DH have negligible variational effects at 300 K, whereas for Cl + H_2 and Cl + HD the variational effects are large. In Fig. 3 classical generalized sum-of-states plots are compared for the smallest- and largest-skew-angle systems, Cl + HD and Cl + DH respectively. At low energies near the classical threshold the minima of these curves are near the saddle point for both systems. The fact that the transverse vibrational frequency for Cl + DH changes more slowly in moving away from the saddle point leads to flatter sum-of-state curves with minima near the saddle point. As a result, as illustrated by Fig. 4, there is a greater difference between TST and μVT for Cl + HD than for Cl + DH.

As a contrast to small-skew-angle reactions involving the transfer of a light atom between heavy atoms, we have also studied the H + BrH and H + BrT systems which have high skew angles of 89.3° and 88.8°, respectively. Although the effects of variational optimization of the dividing surfaces are not as large as in some of the small-skew-angle systems, the increase of the transverse vibrationally frequency upon moving off of the symmetrically located saddle

point leads to 45% and factor-of-3.8 decreases of the generalized transition-state theory rate constant by variational optimization of the dividing surface for H + BrH and H + BrT, respectively, at 300 K. Thus, the small skew angle is not necessary to observe such effects; they may result from the shape of the potential energy surface even for large-skew-angle systems.

Reactions which are highly endoergic (exoergic) tend to have late (early) barriers.[91] The last nine systems listed in Table 3 are highly endoergic or exoergic reactions. The two potential energy surfaces used for the I + H_2 reaction are very similar; both surfaces have saddle points which are located in the interaction region and are extremely low, 0.06 kcal/mol above the bottom of the asymptotic product vibrational well. In the interaction region the transverse vibrational frequency is considerably lower than the product vibrational frequency. Because of the small change in the potential along the MEP in going from the saddle point to products the change in the vibrational frequency locates the CVT dividing surface in the asymptotic product region. The saddle point for the F + H_2 reaction is not quite as far into the interaction region as it is in the H_2I system, and also the intrinsic barrier is higher, 1.06 kcal/mol. Therefore, the entropic factor does not dominate as much in this reaction as for I + H_2 and the variational effects for F + H_2 and F + D_2 are smaller than for I + H_2. The H + F_2 and H + Cl_2 reactions are strongly exoergic with saddle points well into the asymptotic reactant region. For these systems the transverse vibrational frequency is slowly varying along the reaction coordinate near the saddle point and no variational effects are seen.

Finally we note a general feature of Table 3. The location of the CVT transition state at 300 K is very close to the maximum of the adiabatic ground-state potential curve for all 24 systems. This is because at low temperatures the dominant contribution to the canonical rate in the adiabatic theory comes from the ground-state state-selected rate constant. At higher temperatures deviation of the CVT dividing surface location from the location of the maximum of the adiabatic ground-state potential curve will become greater; however, in most cases involving H the ground state dominates up to high temperatures (about 1000-1500 K). Therefore, the most important region of the potential energy surface for performing variational TST calculations is the region around the maximum of the adiabatic ground-state curve.

V. QUANTIZED THREE-DIMENSIONAL REACTIONS AT ROOM TEMPERATURE

Although μVT is the most accurate of the variational theories, its application is computationally the most difficult because of the state counting needed to compute the generalized number of states, $N^{GT}(E,s)$. Comparisons of μVT, CVT, and ICVT for collinear reactions indicate that ICVT can offer much improvement over CVT and can also provide a much more practical method for calculations in three-dimensions than μVT.[23,24] Thus, our applications of VTST to three-dimensional reactions have used CVT[27,33-35] and ICVT.[23,24,36] These applications fall under three general categories: (i) tests of the theory against accurate quantum scattering calculations using a semiempirical potential energy surface[27] or against experiment using an accurate one,[28] (ii) studies of the effects of variational optimization of the dividing surfaces for a wide variety of systems using RMBEBO potential energy surfaces,[33,34] and (iii) adjustment of semiempirical potential energy surfaces such that the VTST calculations reproduce experimental data as well as possible.[36] For three-dimensional reactions we have generally found that the ICVT and CVT predictions are very close. Since CVT is easier to interpret, our discussion here will be limited to CVT calculations in categories (ii) and (iii). We begin with a brief review of the formalism; details of the theory and computational aspects of the calculations can be found in references 23 and 33.

A. Implementation of the Theory for Three-Dimensional Atom-Diatom Reactions

We consider the class of three-dimensional reactions of an atom A with a diatomic BC in which the MEP is collinear. For these cases the MEP is the same as for collinear reactions. The GTST expression for the three-dimensional canonical rate constant is given by equation (4). For these cases the reactants partition function per unit volume is approximated by

$$\Phi^{R}(T) = \Phi_{rel}^{A,BC}(T)\, Q_{str}^{BC}(T)\, Q_{r}^{BC}(T) \tag{39}$$

where $\Phi_{rel}^{A,BC}$ is the reactant relative-translational partition function per unit volume, and $Q_{str}^{BC}(T)$ and $Q_{r}^{BC}(T)$ are the stretching vibrational and rotation partition functions for the BC molecule. Similarly the partition function for the generalized transition state located at s is approximated by the product of terms for the stretching, bending, and rotational degrees of freedom

$$Q^{GT}(T,s) = Q_{str}^{GT}(T,s)\, [Q_{b}^{GT}(T,s)]^{2}\, Q_{r}^{GT}(T,s) \tag{40}$$

where

$$Q^{GT}_{str}(T,s) = \sum_{n=0}^{n_{max}(s)} \exp[-\beta\varepsilon^{GT}_{str}(n,s)] \tag{41}$$

$$Q^{GT}_{b}(T,s) = \sum_{i=0}^{i_{max}} \exp[-\beta\varepsilon^{GT}_{b}(i,s)] \tag{42}$$

$$Q^{GT}_{r}(T,s) = \sum_{J=0}^{\infty} (2J+1)\ \exp[-\beta\hbar^2 J(J+1)/2I(s)] \tag{43}$$

$$I(s) = \{[r_{AB}(s)]^2 m_A m_{BC} + [r_{BC}(s)]^2 m_C m_{AB} + 2r_{AB}(s)\, r_{BC}(s)\, m_A m_{BC}\}/m_{ABC} \tag{44}$$

and $\varepsilon^{GT}_{str}(n,s)$ and $\varepsilon^{GT}_{b}(i,s)$ are the quantized energy levels for the stretching and bending vibrational degrees of freedom, respectively, with the zero of energy chosen at the bottom of the vibrational well at s. The potential energy for the stretching degree of freedom is fit to a Morse potential as in the collinear case. The bending potential is approximated by a mixed harmonic-quartic potential[33,45,79] for which i_{max} is the highest bound state. The harmonic vibrational constants for the stretch and the bend are called $\hbar\omega_{str}$ and $\hbar\omega_{b}$, respectively. Quantization of the bound degrees of freedom is implemented by using anharmonic quantized energy levels in the partition functions.

The conventional TST rate expression is obtained by evaluating $k^{GT}(T,s)$ at $s = 0$ and the CVT rate expression is obtained by evaluating $k^{GT}(T,s)$ at the location $s^{CVT}_{*}(T)$ which minimizes it. In the collinear case the stretching degree of freedom was the only one responsible for moving the CVT transition state off of the saddle point location. For reactions in three dimensions the competition between the energetic and entropic factors now contains contributions from bending and rotational degrees of freedom. As discussed above (section IV) for collinear reactions, the ratio of rate constants $k^{\ddagger}(T)/k^{CVT}(T)$ is the CVT recrossing correction $F^{CVT}(T)$, *i.e.*, it is the CVT estimate of the correction factor that accounts for recrossing of the conventional dividing surface. For a three-dimensional atom-diatom reaction, this recrossing correction is the product of the ratios $F_v(T)$ and $F_r(T)$ of vibrational partition functions and rotational partition functions, each with their zero of energy at the respective location on the MEP, and of the classical Boltzmann factor ratio $F_V(T)$, *i.e.*,

$$F^{CVT}(T) \equiv k^{\ddagger}(T)/k^{CVT}(T) = F_v(T)\, F_r(T)\, F_V(T) \tag{45}$$

where

$$F_r(T) = [Q_r^{\ddagger}(T)/Q_r^{CVT}(T)] \tag{46}$$

and

$$F_V(T) = \exp\left(-\beta\{V_{MEP}(s=0) - V_{MEP}(s=s_*^{CVT}(T))\}\right) \tag{47}$$

and the vibrational factor $F_v(T)$ can further be factored into

$$F_v(T) = F_{str}(T)\, F_b(T) \tag{48}$$

where

$$F_{str}(T) = Q_{str}^{\ddagger}(T)/Q_{str}^{CVT}(T) \tag{49}$$

and

$$F_b(T) = Q_b^{\ddagger}(T)/Q_b^{CVT}(T) \tag{50}$$

In these equations the superscripts ‡ and CVT denote the value of the GT partition function evaluated at $s = 0$ or $s = s_*^{CVT}(T)$, respectively. In the following subsections we shall use the factorization of the CVT recrossing correction as given by equations (45)-(50) to analyze the effects of variational optimization of the GTST dividing surface and how these effects depend on potential energy surface. Notice that the zeroes of energy for the generalized transition state partition functions in equations (4), (5), and (40) are at the local potential minimum $V_{MEP}(s)$ rather than at the local zero point energy. Thus equations (4) and (45)-(50) provide a factorization of the quantized rate constant into classical energetic and classical entropic factors, as opposed to the quantized energetic and quantized entropic factors. In other words, for purposes of interpreting the results, we treat zero point effects as entropic effects rather than energetic effects, although in a strictly quantum mechanical formalism zero-point effects would be energetic effects. As discussed elsewhere,[23,33-35] the method we use including zero point effects with the entropic effects makes it particularly easy to contrast variational and conventional transition state theories. In this language, conventional transition state theory locates the transition state at the highest energy point on the reaction path but variational transition state theory considers the competition of entropic and energetic factors in defining the transition state.

In this chapter we shall not emphasize the results of quantal corrections to the reaction-coordinate motion for three-dimensional collisions. However such corrections may be carried out using essentially the same techniques as discussed above for collinear reactions. In particular, we use adiabatic transmission coefficients obtained by calculating quantal transmission through and across the one-dimensional adiabatic ground-state potential barrier

$$V_a^G(s) = V_{MEP}(s) + \varepsilon_{str}^{GT}(n=0,s) + 2\varepsilon_b^{GT}(i=0,s) \qquad (51)$$

This differs from the collinear expression only in the addition of the contributions from the doubly degenerate bending motion. The $V_a^G(s)$ barrier defined by equation (51) is also useful in interpreting the origin of variational effects when quantal effects are not included on the reaction coordinate, and we shall use it below for this purpose.

B. Survey of Reactions on RMBEBO Potential Energy Surfaces

The RMBEBO model was used to generate a wide variety of potential energy surfaces to study the effects of variational optimization of the dividing surface for various reaction types. This model does not predict quantitatively reliable potential energy surfaces, and we made no attempt to empirically fit any of the potential parameters to experimental data. Instead, we used previously published values for the parameters to generate physically reasonable potential energy surfaces that could then be used in VTST calculations.

In Table 4 we present a review of our studies of the effects of variationally optimizing the dividing surface by CVT for the 300 K rate constant for 14 representative three-dimensional reactions using RMBEBO surfaces. All the reactions are listed in the endoergic or thermoneutral direction, and the systems are listed in order of increasing bond order $n_{AB}^{\ddagger}$ of the new AB bond at the saddle point. (It is not necessary to study exoergic reactions separately since both conventional TST and VTST satisfy detailed balance.) For a bond order $n_{AB}^{\ddagger}$ near zero the saddle point is in the asymptotic reactant region whereas for $n_{AB}^{\ddagger}$ near one the saddle point is in the asymptotic product valley; this agrees with Hammond's postulate.[92] The bond order n_{AB}, the potential along the MEP, and the vibrational frequencies for the stretching and bending degrees of freedom are given at the saddle point and at the CVT dividing surface for 300 K. The location and height of the maximum of the adiabatic ground-state potential curve are also indicated. The ratio of the conventional and CVT rate constants is presented and is decomposed into its contributions from the classical energetic factor [the Boltzmann factor of $V_{MEP}(s)$] and the remaining, or classical entropic, factors. In

Table 4
Generalized-transition-state quantities for three-dimensional reactions with RMBEBO potential energy surfaces at 300 K.

System A + BC	Skew angle (degrees)	ΔE_0 (kcal/mol)	at saddle point					at maximum of adiabatic ground-state barrier		at CVT transition state					comparison of conventional and canonical variational transition state theory				
			n_{AB}	V_{MEP} (kcal/mol)	$\hbar\omega_{str}$ (cm^{-1})	$\hbar\omega_b$ (cm^{-1})	$\Delta V_a^{\ddagger G}$ (kcal/mol)	n_{AB}	ΔV^{AG} (kcal/mol)	n_{AB}	V_{MEP} (kcal/mol)	$\hbar\omega_{str}$ (cm^{-1})	$\hbar\omega_b$ (cm^{-1})	ΔV_a^{CVTG} (kcal/mol)	F_V	F_{str}	F_b	F_r	F^{CVT}
C + HC	23	0.0	0.50	12.7	621	508	10.94	0.37	12.83	0.37	12.1	2364	497	12.83	0.40	65.8	0.94	0.99	24.7
Cl + CCl	42	0.0	0.50	3.6	305	80	3.06	0.34	3.30	0.35	3.4	599	78	3.30	0.74	2.48	0.95	0.99	1.74
C + ClC	75	0.0	0.50	6.2	520	75	5.93	0.5	5.93	0.50	6.2	520	75	5.93	1.00	1.00	1.00	1.00	1.00
C + H_2	47	1.84	0.55	10.7	1759	662	12.88	0.39	14.14	0.40	13.9	3118	673	14.12	0.32	24.5	1.06	0.96	7.94
H + HO	47	6.19	0.62	10.8	3260	603	11.92	0.72	12.34	0.71	10.6	3733	584	12.33	0.73	3.03	0.91	0.95	1.90
Cl + CH	76	22.6	0.85	4.8	761	198	27.81	0.82	27.85	0.81	4.6	857	214	27.83	0.77	1.27	1.18	1.00	1.15
H + HF	46	31.4	0.91	33.0	4279	488	34.62	0.91	34.63	0.90	32.9	4248	515	34.62	0.95	0.93	1.16	1.05	1.08
Li + HO	25	55.4	0.95	62.7	1546	320	60.49	0.93	60.54	0.93	62.6	1603	341	60.54	0.85	1.14	1.16	1.05	1.19
Cl + HO	17	7.2	0.96	8.3	3020	171	8.16	0.92	8.24	0.89	8.4	3053	235	8.20	0.72	1.08	1.82	1.15	1.63
Cl + HF	16	32.5	0.987	34.4	3008	143	33.22	0.98	33.28	0.96	34.2	3035	203	33.22	0.70	1.07	1.89	1.18	1.67
Li + HI	21	16.6	0.991	18.9	1390	172	18.07	0.98	18.10	0.96	18.6	1418	226	18.03	0.67	1.07	1.72	1.20	1.48
Cl + ClH	83	45.0	0.992	0.7	563	69	45.91	0.991	45.91	0.985	0.7	561	83	45.89	0.86	0.99	1.42	1.01	1.22
I + HO	15	38.8	0.994	0.2	2321	112	39.37	0.988	39.42	0.979	0.03	2345	162	39.35	0.71	1.06	1.89	1.18	1.68
I + HBr	8	16.1	0.998	0.1	2311	83	16.52	0.996	16.55	0.989	16.5	2314	139	16.44	0.67	1.01	2.35	1.25	1.98

the collinear reactions the only contribution to the generalized transition-state partition function is from the stretching degree of freedom, whereas for reactions in three dimensions there are contributions to the classical entropic factor from the bending and rotational degrees of freedom as well.

As in the collinear reactions, the symmetric systems with small skew angles have the largest effects of variationally optimizing the location of the dividing surface at room temperature. For symmetric reactions the stretching degree of freedom provides the dominant entropic factor in moving the generalized transition-state dividing surface off the saddle point, and the CVT dividing surfaces for such systems are located to increase the stretching vibrational frequency. This can be understood by examining the energy levels for the various degrees of freedom. The vibrational frequencies, and thus the vibrational energies, of the stretching degree of freedom are much larger than those for the bending degree of freedom. The rotational energy levels are the most closely spaced. The energy levels of the stretching degree of freedom are sufficiently high that at low temperatures the stretching partition functions are dominated by the ground state and the ratio of stretching partition functions for two locations of the GTST dividing surface is approximately given by

$$F_{str}(T) \simeq \exp\left(-\beta\{\varepsilon_{str}(n=0,s=0) - \varepsilon_{str}[n=0,s=s_*^{CVT}(T)]\}\right) \qquad (52)$$

Small differences in the stretching vibrational frequency at the saddle point and CVT dividing surface location can give a large ratio of stretching partition functions. The bending and rotational energy levels are much more closely spaced and to a good approximation these degrees of freedom can often be interpreted classically. In such cases the ratio of bending partition functions is approximated by

$$F_b(T) \simeq \frac{\omega_b(s=s_*^{CVT})}{\omega_b(s=s_0)} \qquad (53)$$

and the ratio of rotational partition functions is approximated by

$$F_r(T) \simeq \frac{I(s=0)}{I(s=s_*^{CVT})} \qquad (54)$$

Thus, in contrast to the stretching degree of freedom, small changes in the bending frequency or moment of inertia do not result in large changes in the ratio of partition functions at low temperatures.

The rotational degree of freedom does not contribute significantly to the ratio of rate constants $F^{CVT}(T)$ at 300 K for any of

the systems in Table 4. The bending degree of freedom plays a more important role, however, for the endoergic systems with saddle points in the asymptotic product region. In these systems the BC bond length at the saddle point is large and the bending motion is very "loose". The bending motion can be tightened by moving the generalized transition state towards the reactant valley. If the saddle point is sufficiently far into the asymptotic product region the stretching frequency will be nearly equal to its asymptotic value and will be slowly varying with respect to the location of the dividing surface. For example, for the I + HO and I + HBr reactions the bending degree of freedom gives the major contribution to the ratio of rate constants $F^{CVT}(T)$ at 300 K.

At low temperatures such as T = 300 K the variational effects are larger for the symmetric systems in which the stretching degree of freedom dominates than for the systems with saddle points in the asymptotic product region where the bending degree of freedom dominates. However, at higher temperatures this trend can reverse as discussed in section V.

C. Survey of Reactions on Other Potential Energy Surfaces

The effect of variationally optimizing the dividing surface has also been investigated for three-dimensional reactions using other analytic functional forms for the potential energy surface. The most popular analytic expressions for global potential energy surfaces are the LEPS and extended LEPS functional forms.[70,71,82] In Table 5 we present our results for a variety of reactions on such surfaces. Information about the surface parameters, quantal endoergicities, and adiabatic ground-state barrier heights are listed in Table 1. In Table 5 the systems are ordered similarly to the order used in Table 4, *i.e.*, the reactions with symmetric saddle points are listed first, followed by those with saddle points progressively further into the product region. As in Tables 3 and 4, the classical potential energy (referenced to the classical equilibrium position of the reactants), the harmonic frequencies for the bound degrees of freedom, and the value of the adiabatic ground-state potential energy curve (referenced to reactant zero point energy) are given for two locations of the dividing surface: the saddle point and the CVT transition state at 300 K. The location and height of the maximum of the ground-state adiabatic potential curve, the ratio $k^{\ddagger}(T)/k^{CVT}(T)$, equal to the CVT recrossing factor $F^{CVT}(T)$, and its factorization into $F_{str}(T)$, $F_b(T)$, $F_r(T)$, and $F_V(T)$ are also given.

The first system in Table 5 is a three-body model[57] of a hydrogen-atom transfer between two methyl groups. The results for the collinear reaction of the same system were included in Table 3. For collinear reaction the stretching degree of freedom competed

Table 5
Generalized-transition-state quantities for three-dimensional reactions with various potential energy surfaces at 300 K.[a]

System A + BC	Surface	Skew angle (degrees)	at saddle point				at maximum of adiabatic ground-state barrier		at CVT transition state					comparison of conventional and canonical variational transition state theory				
			V_{MEP} (kcal/mol)	$\hbar\omega_{str}$ (cm^{-1})	$\hbar\omega_b$ (cm^{-1})	$\Delta V_a^{\ddagger G}$ (kcal/mol)	s_*^{AG} (a_0)	ΔV^{AG} (kcal/mol)	s_*^{CVT} (a_0)	V_{MEP} (kcal/mol)	$\hbar\omega_{str}$ (cm^{-1})	$\hbar\omega_b$ (cm^{-1})	ΔV_a^{CVTG} (kcal/mol)	F_V	F_{str}	F_b	F_r	F^{CVT}
$^{15}C + H^{15}C$	3	20.4	4.49	510	62	3.01	-0.13	3.80	-0.13	3.68	1765	57	3.80	0.25	21.68	0.74	0.98	3.98
I + HI	11	7.2	1.53	146	392	-0.34	-0.32	1.05	-0.23	1.12	1563	314	1.03	0.50	58.1	0.60	0.94	16.5
I + HI	12	7.2	1.35	149	394	-0.57	-0.39	0.94	-0.28	0.96	1662	302	0.92	0.52	72.0	0.55	0.93	18.9
Cl + DH	4	55.8	7.67	1252	563	5.77	-0.20	5.94	-0.19	6.48	2084	623	5.94	0.13	7.21	1.40	0.95	1.29
Cl + HD	4	36.4	7.67	1061	664	5.82	0.15	6.08	0.14	7.04	1937	544	6.08	0.35	8.04	0.53	0.97	1.42
H + BrH	5	89.3	3.95	1821	98	2.78	-0.54	3.39	-0.37	3.88	2079	85	3.35	0.89	1.84	0.81	0.95	1.26
H + BrT	5	88.8	3.95	1487	80	4.11	0.92	4.87	0.68	3.84	2095	70	4.83	0.83	4.21	0.83	0.86	2.48
Cl + CH	13	76.1	31.01	695	109	28.22	-0.005	28.22	-0.02	30.99	693	115	28.20	0.96	0.99	1.10	1.00	1.05
Cl + CH	14	76.1	25.61	827	12	22.71	-0.036	22.71	-0.31	25.34	799	34	22.47	0.64	0.93	3.79	1.09	2.47
Cl + HF	15	16.1	43.72	755	435	38.93	0.090	41.53	0.085	43.30	2057	383	41.53	0.49	22.6	0.73	0.97	7.91
Cl + HF	16	16.1	35.01	2288	383	33.58	0.19	33.77	0.12	34.98	2525	338	33.75	0.94	1.75	0.75	0.96	1.18
Na + ClH	17	84.0	10.61	832	47	7.72	-0.50	8.56	-0.42	10.15	1722	56	8.55	0.46	8.44	1.34	0.86	4.47
Br + HCl	18	11.58	16.69	1437	307	15.42	0.42	16.14	0.24	16.55	2148	226	16.08	0.83	5.38	0.54	0.93	2.25

a. column meanings are as explained in text for Tables 3 and 4; the endoergicities are in Table 1

Table 6
Comparison of stretching frequencies (cm^{-1}) from a molecular orbital calculation and from two model potential energy surfaces.

	PRDDO[a] $H_3{}^{12}C\text{-}H\text{-}{}^{12}CH_3$	ext. LEPS $^{15}C\text{-}H\text{-}^{15}C$	ext. LEPS $^{12}C\text{-}H\text{-}^{12}C$	RMBEBO $^{12}C\text{-}H\text{-}^{12}C$
C-H stretch	3700[b]	2889	2912	2912
C-H-C symmetric stretch	740[c]	510	548	621

a. reference 93

b. C_{3v} $H_3C\text{-}H$ with tetrahedral angles

c. D_{3d} $H_3C\text{-}H\text{-}CH_3$ with tetrahedral angles

well with the classical Boltzmann factor in determining the position of the CVT dividing surface; however, in three dimensions it must compete with the bending degree of freedom, and this lessens displacement of the CVT transition state from the saddle point from 0.134 a_0 to 0.127 a_0. It also lessens the ratio $k^{\ddagger}(T)/k^{CVT}(T)$, although this ratio is still very large for the three-dimensional reaction—a factor of 4 at 300 K. A similar system was studied using the RMBEBO model and is included in Table 4.[33,35] For the RMBEBO case, the ratio $F^{CVT}(T)$ of three-dimensional rate constants is much larger than for the extended LEPS surface because the potential energy along the MEP varies more slowly in the vicinity of the saddle point. Thus, at the CVT surface transition state for the RMBEBO surface, although it is only 0.062 a_0 from the saddle point, the stretching vibrational frequency is 2364 cm^{-1}, which is much larger than the value of 621 cm^{-1} at the saddle point. The corresponding values for extended LEPS system are 1765 cm^{-1} and 510 cm^{-1}. In Table 6 we compare the stretching vibrational frequency for CH in the reactants and for the C-H-C symmetric stretch as calculated[93] for $H_3C\text{-}H\text{-}CH_3$ using the PRDDO molecular orbital method[94] to the values for extended LEPS and RMBEBO model surfaces. This comparison indicates that the model potentials provide a reasonable representation of this system, at least in the saddle point region. Thus the large decrease of the stretching frequency at the saddle point as compared to either reactants or products, which is the crucial feature of the model surfaces that causes them to have large $k^{\ddagger}(T)/k^{CVT}$ values, does not appear to be an artifact of our models.

The I + HI surfaces[83] have symmetrically located saddle points and very small skew angles. These cases, like the case discussed in the previous paragraph, show that the very large effects of variational optimization of the dividing surface seen for the RMBEBO systems with symmetric saddle point locations are not restricted to those types of surfaces.

The collinear reactions for the H + BrH and H + BrT systems[70,79] have $k^{\ddagger}(T)/k^{CVT}(T)$ ratios of 1.83 and 3.84, respectively, at 300 K. Table 5 shows that the effect of the bending degree of freedom on these systems is to decrease these ratios. It also decreases $s_*^{CVT}(T)$, *e.g.*, from 0.54 a_0 for collinear H + BrH to 0.37 a_0 for three-dimensional H + BrH. The situation is similar for the Cl + HD reactions, for which $k^{\ddagger}(T)/k^{CVT}(T)$ decreases from 3.04 to 1.42 and $s_*^{CVT}(T)$ decreases from 0.18 a_0 to 0.14 a_0 in passing from a one-dimensional to a three-dimensional world. In contrast, for the Cl + DH system in which the collinear $k^{\ddagger}(T)/k^{CVT}(T)$ ratio is only 1.01, the three-dimensional ratio is 1.29. Notice that both the stretching and bending degrees of freedom contribute factors of 1.4 or more to this ratio. For Cl + DH, $s_*^{CVT}(T)$ changes from -0.02 a_0 for the collinear reaction to -0.19 a_0 for the three-dimensional reaction.

Results for the Cl + CH system with an RMBEBO surface were included in Table 4, and Table 5 gives results for this system for both LEPS and extended LEPS surfaces. For these two surfaces we use the same set of equilibrium geometries, range parameters, and dissociation energies for the input Morse curves as we did for the RMBEBO surface, and we present results for two sets of Sato parameters. The first choice, a LEPS surface with all Sato parameters zero, yields a saddle point whose location and height are close to those obtained from the RMBEBO surface. The saddle point location is $r_{ClC}^{\ddagger} = 3.42\ a_0$, $r_{CH}^{\ddagger} = 3.22\ a_0$, and the intrinsic barrier height is 5.51 kcal/mol. For the RMBEBO surface the saddle point is located at $r_{ClC}^{\ddagger} = 3.40\ a_0$, $r_{CH}^{\ddagger} = 3.00\ a_0$, and the intrinsic barrier height is 4.78 kcal/mol. For both these surfaces, the Cl-C bond distance at the saddle point is very near its equilibrium value of 3.33 a_0, and the saddle point is well into the product channel. The second choice of Sato parameters, $S_{Cl,C} = S_{Cl,H} = 0.167$, is based on the values that Stern, Persky, and Klein[78] used for Cl + H_2. This leads to an extended LEPS surface which is very different from the two previous surfaces; the saddle point is extremely far into the product channel, $r_{ClC}^{\ddagger} = 3.33\ a_0$ and $r_{CH}^{\ddagger} = 5.14\ a_0$, and the intrinsic barrier height is only 0.11 kcal/mol. Although the LEPS surface resembles the RMBEBO surface more than the extended LEPS surface does, the variational effects on the LEPS and RMBEBO surfaces are quite different. For the RMBEBO surface the effects of the stretching and bending degrees of freedom reinforce each other, but only a small decrease in the rate constant is realized from placing the dividing

surface at the CVT location. On the LEPS surface the stretching and bending degrees of freedom compete, and the $k^{\ddagger}(T)/k^{CVT}(T)$ ratio is closer to unity. For the extended LEPS surface on which the saddle point is well into the asymptotic product region, the location of the CVT dividing surface is dominated by the bending degree of freedom. The tightening of the bending potential contributes a factor of 3.79 toward reducing the rate constant upon moving the dividing surface from the saddle point to the CVT transition state; the resulting $k^{\ddagger}(T)/k^{CVT}(T)$ ratio is 2.47 at 300 K.

The results for the first of the two Cl + HF systems in Table 5 were obtained for a LEPS surface for which the equilibrium geometries, range parameters, and dissociation energies for the input Morse curves are the same as for the RMBEBO surface used for the system listed in Table 4, and all Sato parameters are set to zero. This gives a surface with a more symmetric saddle point than the RMBEBO one, and the intrinsic barrier height is much larger, 9.62 kcal/mol as compared to 0.28 kcal/mol for the RMBEBO surface. For the more symmetric LEPS system, the small skew angle of 16.1 degrees leads to a large contribution (22.6, see Table 5) to the ratio of conventional TST and CVT rate constants from the stretching degree of freedom. The other surface studied for Cl + HF has the parameters of Ding *et al.*[84] This surface has its saddle point further into the product channel than the previous LEPS surface but not as far as the RMBEBO saddle point, and the intrinsic barrier height is 1.08 kcal/mol. In this system the stretching degree of freedom dominates the location of the variational dividing surface, but the competition of the bending degree of freedom makes the CVT dividing surface pass only slightly less flux than the saddle-point one.

The Na + ClH reaction is studied with a potential surface of Polanyi and Sathyamurthy;[85] this surface has a saddle point that is nearly symmetric and the effect of variationally optimizing the dividing surface is to place it more towards reactants. This is a consequence of the fact that the heavy-light mass combination of the initial diatom leads to the reactant stretching frequency being higher than that for the products. The conventional transition-state theory stretching frequency (832 cm^{-1}) is also well below the product stretching frequency (1829 cm^{-1}), but the optimum direction to move the dividing surface is towards reactants. For this reaction moving the dividing surface from the saddle point towards reactants tightens both the stretching and bending vibrational motions and greatly reduces the calculated rate constant.

The final system considered in Table 5 is the Br + HCl reaction for the extended LEPS surface of Douglas *et al.*[86] Although this system has its saddle point well into the product channel, it differs from other systems with this property in that it does not have the location of its variational dividing surface dominated by the bending

Table 7
Kinetic isotope effects for the three-dimensional reactions Cl + AB → ClA + B where A,B = H, D, T. (For homonuclear AB our rates are for reactions with both ends.)

AB/CD	T (K)	k(AB)/k(CD)				
		surface 4		surface 27		experiment[b]
		‡/W[a]	CVT/MCPSAG[b]	‡/W[a]	CVT/MCPSAG[a]	
$H_2/(HD + DH)$	245	3.1	3.1	2.4	2.6	3.4
	345	2.5	2.4	2.1	2.0	2.5
	1000	1.5	1.5	1.4	1.4	
H_2/D_2	245	13.7	7.2	10.4	5.1	14.6
	345	8.0	4.7	6.6	3.5	7.5
	1000	2.3	2.2	2.2	1.8	
H_2/T_2	245	37.3	17.7	26.3	10.1	34.2
	345	21.6	11.4	16.5	6.9	18.3
	1000	3.5	2.5	3.3	2.5	

a. reference 36

b. reference 78

Table 8
Temperature dependence of CVT transition states and of factors controlling the CVT recrossing correction for three-dimensional reactions at 300 K (second line) and 2400 K (third line).

System A + BC	Surface	V^P (kcal/mol)	‡ and CVT transition states: s (a_0)	R_{AB} (a_0)	R_{BC} (a_0)	V_{MEP} (kcal/mol)	$\hbar\omega_{str}$ (cm^{-1})	$\hbar\omega_b$ (cm^{-1})	factors in $k^‡/k^{CVT}$: F_V	F_{str}	F_b	F_r	F^{CVT}
H + F_2	9	-103.54	0.0	3.59	2.72	2.35	787	58					
			0.08	3.51	2.72	2.32	774	63	0.95	0.97	1.14	1.00	1.06
			0.36	3.23	2.75	1.42	735	85	0.82	0.94	1.69	1.01	1.32
T + F_2	9	-103.54	0.0	3.59	2.72	2.35	763	41					
			0.05	3.54	2.72	2.34	746	44	0.98	0.96	1.08	1.01	1.02
			0.25	3.33	2.76	1.91	665	54	0.91	0.87	1.42	1.03	1.16
H + Cl_2	10	-48.64	0.0	4.25	3.81	2.42	524	37					
			0.11	4.14	3.82	2.38	519	41	0.93	0.99	1.17	1.00	1.08
			0.48	3.77	3.84	1.32	509	58	0.79	0.97	1.80	1.01	1.40
O + HI	RMBEBO	-40.80	0.0	4.32	3.05	0.24	2321	112					
			0.59	3.71	3.05	0.03	2345	162	0.71	1.06	1.89	1.18	1.68
			1.24	3.03	3.09	-1.99	2444	247	0.63	1.06	3.09	1.44	2.96
F + H_2	8	-31.75	0.0	2.91	1.44	1.06	3843	452					
			-0.03	2.94	1.44	1.06	3899	438	1.00	1.11	0.92	0.99	1.01
			0.22	2.67	1.48	0.83	3272	575	0.95	0.80	1.43	1.12	1.23
F + D_2	8	-31.75	0.0	2.91	1.44	1.06	2726	320					
			0.01	2.90	1.44	1.06	2715	323	1.00	0.98	1.02	1.00	1.00
			0.24	2.66	1.49	0.80	2280	414	0.95	0.81	1.46	1.13	1.27
F + H_2	RMBEBO	-31.10	0.0	2.95	1.44	1.87	4279	488					
			0.09	2.85	1.45	1.83	4248	515	0.95	0.93	1.16	1.05	1.08
			0.34	2.58	1.50	1.22	4097	590	0.87	0.94	1.35	1.20	1.33

O + H_2	RMBEBO	-5.30	0.0	2.29	1.63	5.48	3260	603					
			-0.11	2.43	1.56	5.30	3733	584	0.73	3.03	0.91	0.95	1.90
			-0.06	2.37	1.59	5.41	3589	593	0.98	1.13	0.98	0.97	1.05
Cl + HC	19	-0.90	0.0	2.91	2.56	23.69	427	591					
			0.00	2.91	2.56	23.69	427	591	1.00	1.00	1.00	1.00	1.00
			0.00	2.91	2.56	23.69	427	591	1.00	1.00	1.00	1.00	1.00
Cl + HC	20	-0.90	0.0	2.76	2.42	5.75	472	588					
			-0.11	3.08	2.14	4.69	1879	533	0.17	31.7	0.75	0.98	3.91
			-0.11	3.08	2.14	4.67	1891	532	0.80	4.21	0.85	0.98	3.01
Cl + HC	21	-0.90	0.0	3.04	2.27	7.64	679	589					
			-0.10	3.24	2.14	7.21	1834	533	0.49	16.2	0.74	0.97	5.68
			-0.10	3.24	2.14	7.21	1838	532	0.91	2.82	0.85	0.97	2.12
$^{15}C + H^{15}C$	3	0.00	0.0	2.43	2.43	4.49	510	62					
			-0.13	2.75	2.16	3.68	1765	57	0.25	21.68	0.74	0.98	3.98
			-0.13	2.75	2.16	3.67	1768	57	0.84	3.61	0.85	0.98	2.53
C + HC	RMBEBO	0.00	0.0	2.40	2.40	12.67	621	508					
			-0.06	2.55	2.29	12.13	2364	497	0.40	65.8	0.94	0.99	24.7
			-0.07	2.56	2.29	12.05	2421	496	0.88	4.21	0.96	0.98	3.49
O + HO	RMBEBO	0.0	0.0	2.16	2.16	4.30	665	354					
			-0.09	2.36	2.01	3.92	3402	336	0.52	18.3	0.90	0.97	8.33
			-0.08	2.33	2.02	4.00	3319	340	0.94	5.79	0.94	0.98	4.99
I + HI	11	0.00	0.0	3.37	3.37	1.53	146	392					
			0.23	3.11	3.85	1.12	1563	314	0.50	58.1	0.60	0.94	16.5
			0.16	3.13	3.75	1.23	1390	316	0.94	9.81	0.79	0.90	6.52
I + HI	12	0.00	0.00	3.37	3.37	1.35	149	395					
			0.28	3.10	3.89	0.96	1662	302	0.52	72.0	0.55	0.93	18.9
			0.17	3.13	3.76	1.09	1430	334	0.95	9.91	0.77	0.89	6.47

C + ClC	RMBEBO	0.00	0.0	3.66	3.66	6.16	520	75					
			0.00	3.66	3.66	6.16	520	75	1.00	1.00	1.00	1.00	1.00
			0.18	3.54	3.83	5.89	595	74	0.95	1.14	0.97	0.99	1.03
D + H_2	25	0.00	0.0	1.76	1.76	9.80	1773	871					
			-0.21	2.01	1.56	8.96	2608	826	0.25	7.20	0.80	0.95	1.35
			-0.20	2.00	1.56	9.00	2574	829	0.85	1.53	0.92	0.95	1.13
T + HD	25	0.0	0.0	1.76	1.76	9.80	1328	817					
			-0.20	2.04	1.53	8.80	2231	759	0.18	8.51	0.75	0.96	1.15
			-0.21	2.05	1.53	8.76	2265	756	0.81	1.79	0.87	0.95	1.20
T + T_2	25	0.0	0.0	1.76	1.76	9.80	1190	526					
			0.00	1.76	1.76	9.80	1190	526	1.00	1.00	1.00	1.00	1.00
			0.00	1.76	1.76	9.80	1190	526	1.00	1.00	1.00	1.00	1.00
T + HR	24	0.0	0.0	3.01	3.01	7.40	257	352					
			0.02	2.98	3.03	7.40	257	352	1.00	1.00	1.00	1.00	1.00
			0.82	1.72	4.34	4.86	629	353	0.59	2.46	1.06	0.91	1.40
Cl + H_2	4	3.01	0.0	2.64	1.88	7.67	1358	710					
			-0.24	2.95	1.52	5.79	2766	747	0.42	2.79	1.24	0.96	1.40
			-0.24	2.95	1.52	5.79	2761	748	0.67	2.21	1.12	0.96	1.59
Cl + D_2	4	3.01	0.0	2.64	1.88	7.67	985	503					
			-0.01	2.66	1.85	7.66	979	510	0.98	0.99	1.04	1.00	1.01
			-0.24	2.95	1.53	5.82	1929	530	0.68	2.04	1.12	0.96	1.47
Cl + T_2	4	3.01	0.0	2.64	1.88	7.67	824	412					
			-0.01	2.65	1.86	7.67	819	417	0.99	0.99	1.03	1.00	1.01
			-0.24	2.95	1.52	5.81	1571	433	0.68	1.96	1.11	0.96	1.41
ClH + D	4	3.01	0.0	2.64	1.88	7.67	1252	563					
			-0.19	2.86	1.58	6.48	2084	623	0.13	7.21	1.40	0.95	1.29
			-0.22	2.89	1.56	6.22	2264	596	0.74	1.90	1.20	0.94	1.58

Cl + HD	4	3.01	0.0	2.64	1.88	7.67	1061	664					
			0.14	2.48	2.15	7.04	1937	544	0.35	8.04	0.53	0.97	1.42
			-0.23	3.00	1.49	5.42	2532	669	0.62	2.57	1.03	0.97	1.61
Cl + H_2	27	3.01	0.0	2.78	1.72	7.71	1496	782					
			-0.18	3.02	1.53	6.88	2739	758	0.25	18.9	0.90	0.94	3.98
			-0.17	3.01	1.53	6.94	2682	762	0.85	1.92	0.97	0.94	1.50
Cl + T_2	27	3.01	0.0	2.78	1.72	7.71	894	453					
			-0.11	2.93	1.58	7.32	1297	455	0.52	2.64	1.01	0.97	1.35
			-0.16	2.99	1.54	7.01	1512	444	0.86	1.73	0.98	0.95	1.38
Cl + HD	27	3.01	0.0	2.78	1.72	7.71	1081	726					
			-0.16	3.04	1.51	6.82	2332	695	0.22	19.5	0.86	0.95	3.60
			-0.16	3.04	1.51	6.82	2333	695	0.83	2.29	0.94	0.95	1.70
Cl + DH	27	3.01	0.0	2.78	1.72	7.71	1488	625					
			-0.16	2.96	1.56	7.15	2288	624	0.40	6.65	1.01	0.94	1.21
			-0.16	2.97	1.56	7.13	2310	623	0.89	1.62	1.01	0.94	1.00
Cl + DH	RMBEBO	3.00	0.0	2.55	2.06	8.00	1521	444					
			-0.21	2.78	1.71	6.73	2452	515	0.12	9.04	1.53	0.97	1.57
			-0.26	2.82	1.67	6.34	2691	518	0.71	1.90	1.33	0.95	1.69
O + H_2	26	2.80	0.0	2.11	1.80	12.49	1533	725					
			-0.02	2.13	1.77	12.46	1545	732	0.96	1.03	1.04	1.00	1.03
			-0.20	2.38	1.51	10.26	2842	717	0.63	2.01	1.00	0.95	1.20
C + H_2	RMBEBO	3.90	0.0	2.36	1.79	14.60	1759	662					
			-0.12	2.52	1.65	13.91	3118	673	0 32	24.5	1.06	0.96	7.94
			-0.13	2.53	1.64	13.83	3178	672	0.85	1.99	1.03	0.96	1.68
Na + ClH	17	7.38	0.0	4.83	2.91	10.61	832	47					
			-0.42	5.25	2.64	10.15	1722	56	0.46	8.44	1.34	0.86	4.47
			-0.41	5.24	2.64	10.17	1709	57	0.91	2.12	1.30	0.86	2.16

Na + ^{19}ClH	23	7.38	0.0	4.83	2.91	10.61	833	49					
			-0.42	5.26	2.64	10.14	1742	58	0.45	8.82	1.33	0.86	4.57
			-0.41	5.24	2.64	10.16	1723	58	0.91	2.14	1.29	0.86	2.17
Cl + HO	RMBEBO	8.30	0.0	2.42	3.56	8.65	3020	171					
			-0.40	2.46	2.92	8.45	3053	235	0.72	1.08	1.82	1.15	1.63
			-0.73	2.55	2.50	7.28	3074	311	0.75	1.02	2.39	1.31	2.41
Br + HCl	18	16.16	0.0	2.78	3.18	16.69	1437	307					
			0.24	2.72	3.48	16.55	2148	226	0.83	5.38	0.54	0.93	2.25
			0.06	2.76	2.76	16.64	1733	283	1.00	1.22	0.89	0.98	1.06
Na + FH	22	17.23	0.0	3.73	2.74	18.84	517	168					
			-0.05	3.75	2.59	18.74	533	195	0.85	1.05	1.34	1.00	1.19
			-0.28	3.91	2.02	15.89	1786	307	0.54	3.61	2.74	0.95	5.06
Li + HI	RMBEBO	17.90	0.0	3.02	5.36	18.85	1390	172					
			-0.74	3.03	4.64	18.62	1418	226	0.67	1.07	1.72	1.20	1.48
			-1.66	3.18	3.66	17.35	1542	320	0.73	1.12	2.72	1.52	3.38
Cl + CH	RMBEBO	25.50	0.0	3.40	3.00	30.28	761	198					
			-0.04	3.43	2.87	30.13	851	213	0.77	1.27	1.17	1.00	1.15
			-0.16	3.53	2.59	28.22	1451	247	0.65	1.95	1.49	0.97	1.82
Cl + CH	13	25.50	0.0	3.42	3.22	31.01	695	109					
			-0.07	3.43	3.16	30.99	693	115	0.96	0.99	1.10	1.00	1.05
			-0.12	3.48	2.86	29.94	706	147	0.80	1.02	1.57	1.00	1.27
Cl + CH	14	25.50	0.0	3.33	5.14	25.61	827	12					
			-0.31	3.34	4.17	25.34	799	34	0.64	0.93	3.79	1.09	2.47
			-0.57	3.38	3.35	23.09	718	80	0.59	0.87	10.3	1.15	6.06
Cl + HF	15	34.10	0.0	2.55	2.58	43.72	755	435					
			0.09	2.45	2.75	43.30	2057	383	0.49	22.6	0.73	0.87	7.91
			0.08	2.45	2.75	43.34	2022	385	0.92	2.82	0.83	0.97	2.11

Cl + HF	16	33.93	0.0	2.47	2.81	35.01	2288	383				
			0.12	2.45	2.95	34.98	2525	338	0.94	1.75	0.75	0.96	1.18
			-0.05	2.48	2.74	35.00	2115	407	1.00	0.91	1.10	1.02	1.02
Cl + HF	RMBEBO	34.10	0.0	2.41	3.88	34.38	3008	143				
			-0.50	2.42	3.36	34.17	3035	203	0.70	1.07	1.89	1.18	1.67
			-1.04	2.46	2.77	32.29	3120	300	0.64	1.05	2.92	1.44	2.84
$I + H_2$	6	35.80	0.0	3.17	2.42	35.87	1320	483				
			0.02	3.15	2.46	35.85	1377	466	0.98	1.15	0.91	1.00	1.01
			-0.05	3.22	2.33	35.75	1212	525	0.98	0.91	1.14	1.01	1.02
Li + HO	RMBEBO	58.70	0.0	3.04	3.28	62.66	1546	320				
			-0.16	3.05	3.11	62.57	1603	341	0.85	1.14	1.16	1.05	1.19
			-0.45	3.08	2.80	61.49	1757	385	0.78	1.15	1.38	1.15	1.43

degree of freedom. Moving the dividing surface further into the product region tightens the stretch while decreasing the bending frequency. Thus the only factor of $F^{CVT}(T)$ that is greater than unity is $F_{str}(T)$.

VI. KINETIC ISOTOPE EFFECTS

Conventional and variational transition state calculations often lead to considerably different predictions for kinetic isotope effects.[27,35,36] This is illustrated for two different potential energy surfaces for Cl + H_2 and isotopic analogs in Table 7, where we have included quantal corrections on the reaction-coordinate motion by the methods discussed in sections II.A and V.A.[36] Because variational transition state theory predicts more accurate kinetic isotope effects than the conventional theory does for collinear reactions, where the predictions have been tested against accurate quantum mechanical dynamics,[21-23,26] and because it is a more internally consistent theory, we prefer to accept its predicted kinetic isotope effects for three-dimensional reactions for any given potential energy surface in preference to those of the conventional theory. For example, since the ‡/W isotope effects in Table 7 agree with experiment better than the CVT/MCPSAG ones do, we conclude that at least part of the good agreement is fortuitous; we suggest that errors in the potential energy surfaces are compensating for errors in the conventional transition-state-theory calculations in this case.

A noteworthy qualitative aspect of variational-transition-state-theory calculations of kinetic isotope effects is that the geometry of the variational transition state may differ for each isotopic variation of a reaction. This means that the usual methods[95] of predicting isotope effects, based on the simplifications possible when nuclear masses are changed with fixed force fields, do not apply. Instead of using such simplifications, we perform completely independent variational calculations for each isotopic case.

VII. TEMPERATURE DEPENDENCES OF BOTTLENECK LOCATIONS AND VARIATIONAL FACTORS FOR QUANTIZED THREE-DIMENSIONAL REACTIONS; HIGH-TEMPERATURE REACTIONS

Table 8 shows how the location of the CVT transition state, the four factors $F_{str}(T)$, $F_b(T)$, $F_r(T)$, and $F_V(T)$, and the $k^{\ddagger}(T)/k^{CVT}(T)$ ratio change as the temperature is increased from 300 K to 2400 K for most of the systems of Tables 4 and 5 plus some others. Although the table shows that the location of the CVT transition state does often change with temperature, the typical trends can be understood by simple arguments for prototype cases in which the temperature dependence of $s_*^{CVT}(T)$ need not be mentioned. For a fixed dividing-

surface location s_* the Boltzmann factor, $\exp\{-\beta[V_{MEP}(s=0) - V_{MEP}(s_*)]\}$, is an increasing function of temperature. Approximating the ratio of stretching partition functions by $\exp\{-\beta[\epsilon_{str}(n=0,s=0) - \epsilon_{str}(n=0,s_*)]\}$ we see that it is a decreasing function of temperature for the common case $\epsilon_{str}(n=0,s=0) < \epsilon_{str}(n=0,s=s_*^{CVT})$. Since the stretching degree of freedom strongly dominates the $k^{\ddagger}(T)/k^{CVT}(T)$ ratio of symmetric systems, this ratio is also a decreasing function of temperature in this case. For example, consider the symmetric C + HC reaction; for this reaction $k^{\ddagger}(T)/k^{CVT}(T)$ decreases with temperature and is 24.7, 6.12, and 3.49 at 300, 600, and 2400 K, respectively. For s_* fixed the ratio of bending partition functions is approximated by $\omega_b(s_*)/\omega_b(s=0)$ and is nearly constant; therefore, when the product of this factor and the Boltzmann factor are the dominant contributions to $k^{\ddagger}(T)/k^{CVT}(T)$, it increases with the temperature. The I + HBr reaction is an example of an endoergic reaction which has its saddle point far into the asymptotic product region. For this system the bending degree of freedom dominates $k^{\ddagger}(T)/k^{CVT}(T)$, and this ratio has the values 1.98, 2.44, and 4.19 at 300, 600, and 2400 K, respectively. These two examples are typical cases, and the trends for most of the other cases can be understood by the same kinds of arguments.

VIII. CONCLUDING REMARKS

The results discussed in this chapter show that the rate constant calculated by applying the transition state assumption at the dynamical bottleneck for a reaction is often quite different from that calculated by conventional transition state theory. Thus it is necessary to understand the properties of potential energy surfaces in bottleneck regions as well as near saddle points. In this chapter we have discussed some of the systematics of potential energy surfaces that are responsible for the location of the bottleneck regions, and we have given many numerical examples. In many cases one can estimate, based on the experience gained from these calculations, what kind and size of effects will be important for a reaction with given saddle point properties and masses. This should make it easier to search for the bottleneck region without having to calculate the whole potential energy surface.

IX. ACKNOWLEDGMENT

This work was supported in part by the U.S. Department of Energy. Office of Basic Energy Sciences, through contract no. DE-AC02-79ER10425.

X. REFERENCES

1. S. Glasstone, K. J. Laidler, and H. Eyring, "Theory of Rate Processes", McGraw-Hill, New York (1941); H. S. Johnston, "Gas Phase Reaction Rate Theory", Ronald Press, New York (1966); D. L. Bunker, "Theory of Gas Phase Reaction Rates", Pergamon Press, Oxford (1966); K. J. Laidler, "Theories of Chemical Reaction Rates", McGraw-Hill, New York (1969).
2. E. Wigner, Calculation of the rate of elementary association reactions, J. Chem. Phys. 5: 720 (1937).
3. J. Horiuti, On the statistical mechanical treatment of the absolute rate of chemical reaction, Bull. Chem. Soc. Japan 13: 210 (1938).
4. J. C. Keck, Variational theory of chemical reaction rates applied to three-body recombinations, J. Chem. Phys. 32: 1035 (1960).
5. J. C. Keck, Variational theory of reaction rates, Advan. Chem. Phys. 13: 85 (1967).
6. P. Pechukas, Statistical approximations in collision theory, in: "Dynamics of Molecular Collisions, Part B", W. H. Miller, ed., Plenum, New York (1976), p. 269.
7. E. Pollak and P. Pechukas, Transition states, trapped trajectories, and classical bound states embedded in the continuum, J. Chem. Phys. 69: 1218 (1978).
8. B. C. Garrett and D. G. Truhlar, Criterion of minimum state density in the transition state theory of bimolecular reactions, J. Chem. Phys. 70: 1593 (1979).
9. B. C. Garrett and D. G. Truhlar, Generalized transition state theory. Classical mechanical theory and applications to collinear reactions of hydrogen molecules, J. Phys. Chem. 83: 1052, 3058(E) (1979).
10. K. Morokuma and M. Karplus, Collision dynamics and the statistical theories of chemical reactions. II. Comparison of reaction probabilities, J. Chem. Phys. 55: 63 (1971).
11. G. W. Koeppl and M. Karplus, Comparison of 3D classical trajectory and transition-state theory reaction cross sections, J. Chem. Phys. 55: 4667 (1971).
12. P. Pechukas and F. J. McLafferty, On transition-state theory and the classical mechanics of collinear collisions, J. Chem. Phys. 58: 1622 (1973).
13. S. Chapman, S. M. Hornstein, and W. H. Miller, Accuracy of transition state theory for the threshold of chemical reactions with activation energy. Collinear and three-dimensional $H + H_2$, J. Amer. Chem. Soc. 97: 892 (1975).
14. W. J. Chesnavich, On the threshold behavior of collinear bimolecular exchange reactions, Chem. Phys. Lett. 53: 300 (1978).
15. B. C. Garrett and D. G. Truhlar, Improved canonical variational theory for chemical reaction rates. Classical mechanical theory and applications to collinear reactions, J. Phys. Chem. 84: 805 (1980).

16. E. Wigner, The transition state method, Trans. Faraday Soc. 34: 29 (1938).
17. W. H. Miller, Quantum mechanical transition state theory and a new semiclassical model for reaction rate constants, J. Chem. Phys. 61: 1823 (1974).
18. W. H. Miller, Semiclassical limit of quantum mechanical transition state theory for nonseparable systems, J. Chem. Phys. 62: 1899 (1975).
19. W. H. Miller, Path integral representation of the reaction rate constant in quantum mechanical transition state theory, J. Chem. Phys. 63: 1166 (1975).
20. D. G. Truhlar, Accuracy of trajectory calculations and transition state theory for thermal rate constants of atom transfer reactions, J. Phys. Chem. 83: 188 (1979).
21. B. C. Garrett and D. G. Truhlar, Accuracy of tunneling corrections to transition state theory for thermal rate constants of atom transfer reactions, J. Phys. Chem. 83: 200, 3058(E) (1979).
22. B. C. Garrett and D. G. Truhlar, Generalized transition state theory. Quantum effects for collinear reactions of hydrogen molecules and isotopically substituted hydrogen molecules, J. Phys. Chem. 83: 1079 (1979); 84: 682(E) (1980).
23. B. C. Garrett, D. G. Truhlar, R. S. Grev, and A. W. Magnuson, Improved treatment of threshold contributions in variational transition-state theory, J. Phys. Chem. 84: 1730 (1980).
24. B. C. Garrett, D. G. Truhlar, and R. S. Grev, Applications of variational transition-state theory and the unified statistical model to $H + Cl_2 \rightarrow HCl + Cl$, J. Phys. Chem. 84: 1749 (1980).
25. B. C. Garrett, D. G. Truhlar, R. S. Grev, and R. B. Walker, Comparison of variational transition state theory and the unified statistical model with vibrationally adiabatic transmission coefficients to accurate collinear rate constants for $T + HD \rightarrow TH + D$, J. Chem. Phys. 73: 235 (1980).
26. B. C. Garrett, D. G. Truhlar, R. S. Grev, A. W. Magnuson, and J. N. L. Connor, Variational transition state theory, vibrationally adiabatic transmission coefficients, and the unified statistical model tested against accurate quantum rate constants for collinear $F + H_2$, $H + F_2$, and isotopic analogs, J. Chem. Phys. 73: 1721 (1980).
27. B. C. Garrett and D. G. Truhlar, Generalized transition state theory calculations for the reactions $D + H_2$ and $H + D_2$ using an accurate potential energy surface: Explanation of the kinetic isotope effect, J. Chem. Phys. 72: 3460 (1980).
28. B. C. Garrett and D. G. Truhlar, Reliable *ab initio* calculation of a chemical reaction rate and a kinetic isotope effect: $H + H_2$ and $^2H + {}^2H_2$, Proc. Natl. Acad. Sci. USA 76: 4755 (1979).
29. B. Liu, *Ab initio* potential energy surface for linear H_3, J. Chem. Phys. 58: 1925 (1973).
30. P. Siegbahn and B. Liu, An accurate three-dimensional potential energy surface for H_3, J. Chem. Phys. 68: 2457 (1978).

31. D. G. Truhlar and C. J. Horowitz, Functional representation of Liu and Siegbahn's accurate *ab initio* potential energy calculations for H + H_2, J. Chem. Phys. 68: 2466 (1978); 71: 1514(E) (1979).
32. D. G. Truhlar and B. C. Garrett, Variational transition state theory, Acc. Chem. Res. 13: 440 (1980).
33. B. C. Garrett and D. G. Truhlar, Generalized transition state theory. Bond-energy-bond-order method for canonical variational calculations with applications to hydrogen atom transfer reactions, J. Amer. Chem. Soc. 101: 4534 (1979).
34. B. C. Garrett and D. G. Truhlar, Generalized transition state theory. Canonical variational calculations using the bond-energy-bond-order method for bimolecular reactions of combustion products, J. Amer. Chem. Soc. 101: 5207 (1979).
35. B. C. Garrett and D. G. Truhlar, Variational transition state theory. Primary kinetic isotope effects for atom transfer reactions, J. Amer. Chem. Soc. 102: 2559 (1980).
36. B. C. Garrett, D. G. Truhlar, and A. W. Magnuson, Variational transition state theory and vibrationally adiabatic transmission coefficients for the kinetic isotope effects in the Cl-H-H reaction system, J. Chem. Phys. 74: 1029 (1981).
37. S. Chapman, B. C. Garrett, and W. H. Miller, Semiclassical transition state theory for nonseparable systems: Application to the collinear H + H_2 reaction, J. Chem. Phys. 63: 2710 (1975).
38. See also H. S. Johnston and D. Rapp, Large tunneling corrections in chemical reaction rates. II, J. Amer. Chem. Soc. 83: 1 (1961) and reference 39.
39. E. Wigner, Über das Überschreiten von Potentialschwellen bei chemischen Reaktionen, Z. Phys. Chem. B 19: 203 (1932).
40. D. G. Truhlar and A. Kuppermann, Exact tunneling calculations, J. Amer. Chem. Soc. 93: 1840 (1971).
41. D. G. Truhlar, The adiabatic theory of chemical reactions, J. Chem. Phys. 53: 2041 (1970), and references therein.
42. R. A. Marcus and M. E. Coltrin, A new tunneling path for reactions such as H + H_2 → H + H, J. Chem. Phys. 67: 2609 (1977).
43. For a review see P. Pulay, Direct use of the gradient for investigating molecular energy surfaces, in: "Applications of Electronic Structure Theory", H. F. Schaefer, ed., Plenum, New York (1977), p. 153.
44. J. A. Pople, R. Krishnan, H. B. Schlegel, and J. S. Binkeley, Derivative studies in Hartree-Fock and Møller-Plesset theories, Int. J. Quantum Chem. Symp. 13: 255 (1979).
45. B. C. Garrett and D. G. Truhlar, Importance of quartic anharmonicity for bending partition functions in transition state theory, J. Phys. Chem. 83: 1915 (1979).
46. For further discussion see D. G. Truhlar, discussion remarks, J. Phys. Chem. 83: 199 (1979).
47. R. L. Jaffe, J. M. Henry, and J. B. Anderson, Variational theory of reaction rates: Application to F + H_2 ⇌ FH + H, J. Chem. Phys. 59: 1128 (1973).

48. G. W. Koeppl, Alternative locations for the dividing surface of transition state theory. Implications for application of the theory, J. Amer. Chem. Soc. 96: 6539 (1974).
49. W. H. Miller, Unified statistical model for "complex" and "direct" reaction mechanisms, J. Chem. Phys. 65: 2216 (1976).
50. G. Koeppl, progress report for Alfred P. Sloan Fellowship for Basic Research, Nov. 9, 1977 (unpublished).
51. E. Pollak and P. Pechukas, Unified statistical model for "complex" and "direct" reaction mechanisms: A test of the collinear $H + H_2$ exchange reaction, J. Chem. Phys. 70: 325 (1979).
52. P. Pechukas and E. Pollak, Classical transition state theory is exact if the transition state is unique, J. Chem. Phys. 71: 2062 (1979).
53. J. P. Davis, A combined dynamical-statistical approach to calculating rates of complex bimolecular exchange reactions, J. Chem. Phys. 71: 5206 (1979).
54. J. P. Davis, A combined statistical-dynamical approach to calculating rates of complex bimolecular exchange reactions: Asymmetric systems, J. Chem. Phys. 73: 2010 (1980).
55. W. J. Chesnavich, T. Su, and M. T. Bowers, Ion-dipole collisions: Recent theoretical advances, in: "Kinetics of Ion-Molecule Reactions", P. Ausloos, ed., Plenum, New York (1979), p. 31.
56. W. J. Chesnavich, T. Su, and M. T. Bowers, Collisions in a noncentral field: A variational and trajectory investigation of ion-dipole capture, J. Chem. Phys. 72: 2641 (1980).
57. B. C. Garrett and D. G. Truhlar, Improved canonical variational theory for chemical reaction rates. Classical mechanical theory and applications to collinear reactions, J. Phys. Chem. 84: 805 (1980).
58. E. Pollak, M. S. Child, and P. Pechukas, Classical transition state theory: A lower bound to the reaction probability, J. Chem. Phys. 72: 1669 (1980).
59. E. Pollak and R. D. Levine, Statistical theories for molecular collisions: A maximum entropy derivation, J. Chem. Phys. 72: 2990 (1980).
60. J. B. Anderson, Statistical theories of chemical reactions. Distributions in the transition region, J. Chem. Phys. 58: 4684 (1973).
61. B. C. Garrett and D. G. Truhlar, unpublished.
62. E. K. Grimmelman and L. L. Lohr, On the exactness of classical transition state theory for collinear reactions, Chem. Phys. Lett. 48: 487 (1977).
63. D. I. Sverdlik and G. W. Koeppl, An energy limit of transition state theory, Chem. Phys. Lett. 59: 449 (1978).
64. D. I. Sverdlik, G. P. Stein, and G. W. Koeppl, The accuracy of transition state theory in its absolute rate theory and variational formulations, Chem. Phys. Lett. 67: 87 (1979).
65. D. Martin and L. M. Raff, A general procedure for classical variational rate calculations for three-body exchange reactions, J. Chem. Phys., submitted for publication.

66. D. G. Truhlar and A. Kuppermann, Exact and approximate quantum mechanical reaction probabilities and rate constants for the collinear H + H_2 reaction, J. Chem. Phys. 56: 2232 (1972).
67. J. Troe, Unimolecular reactions, Int. Rev. Sci., Phys. Chem., Ser. Two 9: 1 (1976).
68. M. Quack and J. Troe, Unimolecular reactions and energy transfer of highly excited molecules, Specialist Periodical Reports Chem. Soc., Gas Kinetics and Energy Transfer 2: 175 (1977), and references therein.
69. W. J. Chesnavich, L. Bass, T. Su, and M. T. Bowers, Multiple transition states in unimolecular reactions: A transition state switching model. Application to the $C_4H_8^+$ system, preprint.
70. C. A. Parr and D. G. Truhlar, Potential energy surfaces for atom transfer reactions involving hydrogens and halogens, J. Chem. Phys. 75: 1844 (1971).
71. D. G. Truhlar and R. E. Wyatt, H + H_2: Potential energy surfaces and elastic and inelastic scattering, Advan. Chem. Phys. 36: 141 (1977).
72. F. T. Wall and R. N. Porter, General potential-energy function for exchange reactions, J. Chem. Phys. 36: 3256 (1962).
73. J. W. Duff and D. G. Truhlar, Effect of curvature of the reaction path on dynamic effects in endothermic reactions and product energies in exothermic reactions, J. Chem. Phys. 62: 2477 (1975).
74. R. N. Porter and M. Karplus, Potential energy surface for H_3, J. Chem. Phys. 40: 1105 (1964).
75. L. M. Raff. L. Stivers, R. N. Porter, D. L. Thompson, and L. B. Sims, Semiempirical VB calculation of the (H_2I_2) interaction potential, J. Chem. Phys. 52: 3449 (1970); 58: 1271(E) (1973).
76. H. S. Johnston and C. A. Parr, Activation energies from bond energies. I. Hydrogen transfer reactions, J. Amer. Chem. Soc. 85: 2544 (1963).
77. S. W. Mayer, L. Schieler, and H. S. Johnston, Computation of high-temperature rate constants for bimolecular reactions of combustion products, Eleventh Symp. (Int.) Combustion 837 (1967).
78. M. J. Stern, A. Persky, and F. S. Klein, Force field and tunneling effects in the H-H-Cl reaction system. Determination from kinetic isotope effect measurements, J. Chem. Phys. 58: 5697 (1973).
79. C. A. Parr, Ph.D. thesis, California Institute of Technology, Pasadena, 1968; C. A. Parr and A. Kuppermann, unpublished.
80. J. T. Muckerman, Applications of classical trajectory techniques to reactive scattering, Theoret. Chem.: Advan. Perspectives 6A: 1 (1981).
81. N. Jonathan, S. Okuda, and D. Timlin, Initial vibrational energy distributions determined by infrared chemiluminescence. III. Experimental results and classical trajectory calculations for the H + F_2 system, Mol. Phys. 24: 1143 (1972).

82. P. J. Kuntz, E. M. Nemeth, J. C. Polanyi, S. D. Rosner, and C. E. Young, Energy distribution among products of exothermic reactions. II. Repulsive, mixed, and attractive energy release, J. Chem. Phys. 44: 1168 (1968).
83. J. A. Kaye and A. Kuppermann, Chem. Phys. Lett. 77: 573 (1981).
84. A. M. G. Ding, L. J. Kirsch, D. S. Perry, J. C. Polanyi, and J. L. Schreiber, Effect of changing reagent energy on reaction probability and product energy distribution, Faraday Disc. Chem. Soc. 55: 252 (1973).
85. J. C. Polanyi and N. Sathyamurthy, Location of energy barriers. VII. Sudden and gradual late-energy barriers, Chem. Phys. 33: 287 (1978).
86. D. J. Douglas, J. C. Polanyi, and J. J. Sloan, Effect of changing reagent energy on reaction dynamics. VI. Dependence of reaction rates on vibrational energy excitation in substantially endothermic reactions, XH(v') + Y → X + HY, Chem. Phys. 13: 15 (1976) (1976).
87. P. J. Kuntz, E. M. Nemeth, J. C. Polanyi, and W. H. Wong, Distribution of reaction products. VI. Hot-atom reactions, T + HR, J. Chem. Phys. 52: 4654 (1970).
88. T. Valencich, J. Hsieh, J. Kwan, T. Stewart, and T. Lenhardt, Simulation of the effects of translational and vibrational energy on H and D atom reactions with HCl and DCl, Ber. Bunsenges. Phys. Chem. 81: 131 (1977).
89. B. R. Johnson and N. W. Winter, Classical trajectory study of the effect of vibrational energy on the reaction of molecular hydrogen with atomic oxygen, J. Chem. Phys. 66: 4116 (1967).
90. M. Baer, An exact quantum mechanical study of the isotopic collinear reactive systems H_2 + Cl and D_2 + Cl, Mol. Phys. 27: 1429 (1974).
91. See, *e.g.*, H. Eyring, S. H. Lin, and S. M. Lin, "Basic Chemical Kinetics", John Wiley & Sons, New York (1980), p. 145.
92. G. S. Hammond, A correlation of reaction rates, J. Amer. Chem. Soc. 77: 334 (1955).
93. R. A. Eades and D. A. Dixon, personal communication.
94. T. A. Halgren and W. N. Lipscomb, Self-consistent-field wavefunctions for complex molecules. The approximation of partial retention of diatomic differential overlap, J. Chem. Phys. 58: 1569 (1973).
95. See, *e.g.*, L. Melander and W. H. Saunders, Jr., "Reaction Rates of Isotopic Molecules", John Wiley & Sons, New York (1980).